UTILIZING FOUR DIMENSIONAL LIGHTNING AND DUAL-POLARIZATION RADAR TO DEVELOP LIGHTNING INITIATION FORECAST GUIDANCE

THESIS

Andrew J. Travis, Captain, USAF

AFIT-ENP-MS-15-M-092

DEPARTMENT OF THE AIR FORCE
AIR UNIVERSITY

AIR FORCE INSTITUTE OF TECHNOLOGY

Wright-Patterson Air Force Base, Ohio

AFIT-ENP-MS-15-M-092

UTILIZING FOUR DIMENSIONAL LIGHTNING AND DUAL-POLARIZATION RADAR TO DEVELOP LIGHTNING INITIATION FORECAST GUIDANCE

THESIS

Presented to the Faculty

Department of Engineering Physics

Graduate School of Engineering and Management

Air Force Institute of Technology

Air University

Air Education and Training Command

in Partial Fulfillment of the Requirements for the

Degree of Master of Science in Applied Physics

Andrew J. Travis, M.S.

Captain, USAF

March 12, 2015

AFIT-ENP-MS-15-M-092

UTILIZING FOUR DIMENSIONAL LIGHTNING AND DUAL-POLARIZATION RADAR TO DEVELOP LIGHTNING INITIATION FORECAST GUIDANCE

THESIS

Andrew J. Travis, M.S.
Captain, USAF

Committee Membership:

Lt Col Robert S. Wacker, PhD
Chair

Lt Col Kevin S. Bartlett, PhD
Member

William F. Bailey, PhD
Member

Abstract

Lightning initiation is a major forecast challenge faced by Air Force's 45th Weather Squadron (45 WS), which provides weather support to Cape Canaveral Air Force Station and Kennedy Space Center (KSC). Prior studies by Thurmond (2014) and Woodard (2011) have shown that dual-polarization (DP) radar can be used to identify the presence of hydrometeors indicative of cloud charging, leading to improved lightning initiation forecasts. The 45 WS currently employs empirical lightning initiation forecast rules which state that in-cloud lightning is likely when radar reflectivity meets or exceeds 37.0 dBZ above the $-10°$C height. This study examined 249 convective cells from March 2012 to March 2014 in order to incorporate DP parameters into existing forecast principles. In-cloud and cloud-to-ground lightning flash data were obtained from the KSC Four Dimensional Lightning Surveillance System, and DP radar data were obtained from the Melbourne, Florida WSR-88D radar. Lightning initiation forecast lead times, probabilities of detection, and false alarm rates were compared between 18 candidate DP-based forecast techniques and current techniques employed by 45 WS. Of the 18 DP-based techniques tested, five outperformed existing techniques based on forecast skill scores, but the overall improvements were limited.

Acknowledgements

It would have been impossible to complete AFIT without the love and support of my wife and son. Thank you for your patience and sacrifice over the past two years. I look forward to moving onto our next assignment together and having more free time to spend with both of you. Thank you to the rest of my family as well. It was great being in Ohio, which allowed for several visits to New York and New Hampshire.

I would also like to thank my professors here at AFIT, especially my advisors Lt Col Wacker, Lt Col Bartlett, and Dr. Bailey. Everything you taught me will help me immensely in the future, and I am grateful to each of you for guiding me through my thesis, my classes, and the entire AFIT journey. Additionally, my thesis could not have been completed without the assistance of Mr. William Roeder at 45th Weather Squadron.

Finally, I'd like to thank my classmates, particularly Dave and Brandon who faced the AFIT struggles and challenges alongside me. It was always helpful to have someone help lift my spirits after a lengthy MATLAB® project or help me out when I got stuck. Good luck to all my classmates at your next assignments, and hopefully we'll run into each other at some point in the future.

Andrew J. Travis

Table of Contents

Page

List of Figures

Figure Page

List of Tables

UTILIZING FOUR DIMENSIONAL LIGHTNING AND
DUAL-POLARIZATION RADAR TO DEVELOP LIGHTNING
INITIATION FORECAST GUIDANCE

I. Introduction

1.1 Motivation

Lightning onset and cessation are major forecast challenges for the Air Force's 45th Weather Squadron (45 WS). The 45 WS mission is to exploit the weather to assure safe access to air and space by supporting operations at Cape Canaveral Air Force Station (CCAFS), Kennedy Space Center (KSC), and Patrick Air Force Base (PAFB). Those locations serve as America's gateway to exploring and utilizing space by facilitating up to 20 launches per year by National Aeronautics and Space Administration (NASA), the Department of Defense (DoD), and commercial customers (NASA 2014). In addition to direct launch support, 45 WS issues severe weather and lightning advisories around-the-clock for 10 different warning circles with radii of 5 or 6 nm centered on areas of operational sensitivity (Roeder et al. 2014). Exploiting the most accurate lightning onset and cessation prediction methods is vital to safeguarding those sensitive areas, which include over $20 billion in equipment, facilities, and 25 000 personnel. Timely and accurate forecasts also avoid wasted time and money caused by false alarms or leaving an advisory valid longer than necessary.

Each year, 45 WS issues an average of 2500 lightning advisories, though this number may decline slightly in the future due to streamlining the number of warning circles from 10 to 13 in May 2014 (Roeder et al. 2014). 45 WS issues two tiers of

lightning advisories, a Phase-1 Lightning Watch and a Phase-2 Lightning Warning. Forecasters issue a watch when lightning is expected within a warning circle within the next 30 min. A watch is issued 30 min prior to when lightning is expected in order to give operators adequate lead time to prepare for a thunderstorm. A warning is issued when lightning is imminent or occurring within one of the circles. Warnings are issued when either lightning aloft or cloud-to-ground (CG) lightning is detected or imminent.

The high frequency of lightning advisories is a consequence of Florida being the lightning capital of the United States. Based on National Lightning Detection Network (NLDN) climatology from 1997–2011, regions of Central and Southern Florida, including the area around CCAFS and KSC, experience over 14 CG lightning flashes per square km per year (Vaisala 2013). The elevated lightning density over Florida is primarily due to favorable regional conditions that permit a significant number of airmass thunderstorms to occur throughout the year.

Locally developing airmass thunderstorms are the most challenging lightning events for 45 WS to forecast. Frequently, small convective cells develop directly over an area of operational sensitivity. This convection may just become a brief rain shower that never produces lightning, or it can develop into a thunderstorm. Using weather radar and other tools, 45 WS forecasters must determine if lightning will occur and when to issue a lightning watch or warning, but these difficult forecasts can lead to numerous false alarms or advisories that do not meet desired lead time. Thunderstorms that form outside the areas of operation sensitivity and advect into the area are typically much easier to forecast since their tracks and timing depend primarily on interrogating the steering flow aloft.

1.2 Historical Lightning Impacts

Space launch missions from KSC/CCAFS have been impacted by lightning since the beginning of the space program. In November 1969, the Apollo 12 Saturn V was struck twice by triggered lightning during liftoff. Triggered lightning occurs when a rocket and its exhaust gases amplify existing electric fields and act as a conductor between charges in the atmosphere and the ground. This triggered event caused power supply and telemetry errors to the launch vehicle that nearly forced the second moon landing mission to be aborted (Starr et al. 1993). In 1975, lightning struck the processing facility containing the Viking 1 orbiter, causing substantial damage. Another triggered lightning event occurred in 1987 when an Atlas Centaur launch vehicle was struck, resulting in a total loss of the rocket and payload. These significant lightning events, along with numerous minor ones, resulted in the strong emphasis that the 45 WS places on lightning monitoring, detection, and sensitive facility protection.

In addition to space launch impacts, lightning causes numerous fatalities and monetary damages each year in the United States. Since 2004, lightning caused an average of 234 injuries and 33 deaths per year, with Florida accounting for the most in any one state (NOAA 2014). Lightning also caused insured property losses of $673.5 million in 2013, with an average claim amount of $5.87k (Insurance Information Institute 2014). The addition of non-insured losses and lost productivity due to suspending or delaying lightning sensitive activities causes the overall yearly economic impact of lightning to be several billion dollars per year.

1.3 Existing Lightning Forecast Methods

New forecasters arriving at 45 WS typically have at least three years of forecasting experience for various regions around the world. As part of newcomer training

covering specific forecast challenges associated with the space program and the East-Central Florida region, 45 WS developed a computer-based training (CBT) entitled Basic Orientation and Lightning Training (BOLT). The CBT was last updated in 2007 and includes nine lessons which discuss the physics of lightning, the different lightning detection methods used by 45 WS, and forecasting techniques.

The forecasting lesson describes how to utilize radar reflectivity from either the WSR-88D radar at the Melbourne, Florida airport (KMLB) or the local WSR-74 at PAFB to predict when lightning initiation or cessation is likely with an airmass thunderstorm based on a set of conditions developed by Pinder in the early 1990s while he worked as a forecaster and Deputy Launch Weather Officer at 45 WS (Roeder and Pinder 1998). Table 1 contains the Pinder Principles for lightning cessation and six different lightning onset scenarios.

Table 1. Pinder Principles for lightning initiation and cessation using weather radar. Table adapted from Roeder and Pinder (1998).

Phenomena	Lightning Type	Radar Intensity	Thermal Level	Vertical Depth
Convective Cell	In-Cloud	$37.0 - 44.0$ dBZ	$\geq -10°$C	≥ 3000 ft
Convective Cell	Cloud-to-Groud	$45.0 - 48.0$ dBZ	$\geq -10°$C	≥ 3000 ft
Anvil Cloud	In-Cloud	≥ 23.0 dBZ	$\geq -10°$C	≥ 3000 ft
Anvil Cloud	Cloud-to-Groud	≥ 34.0 dBZ	$\geq -10°$C	≥ 3000 ft
Debris Cloud	In-Cloud	$23.0 - 44.0$ dBZ	$\geq -10°$C	Variable
Debris Cloud	Cloud-to-Groud	$45.0 - 48.0$ dBZ	N/A	N/A
Cessation	All Types	When above conditions no longer exist.		

1.4 Research Objective

Due to the high frequency of lightning advisories issued by 45 WS and the impact lightning has on operations, it is crucial to advance their existing forecasting techniques. On 27 January 2012, the KMLB WSR-88D upgraded to dual-polarization (DP) capability (NOAA 2012), providing new parameters to include in lightning initiation studies. Thurmond (2014) conducted initial research using DP at KSC/C-

CAFS and showed promising results. The purpose of this research is to build upon the Thurmond (2014) study in order to develop guidance that outperforms a baseline provided by the Pinder Principles. By examining WSR-88D reflectivity and DP products during the early stages of convective development, this study aims to increase lightning forecast lead times and lower the number of false alarms beyond what the baseline methods provide.

1.5 Preview

This chapter introduced the scope of the problem, and touched on working to improve existing 45 WS lightning forecast methods. Chapter II provides a background of the instruments being utilized for this study. It also examines airmass thunderstorm development, lightning initiation, and relevant research already conducted. Chapter III explains the methodology and archived data used to develop results. Chapter IV details data analysis and research results, followed by Chapter V, which discusses the conclusions and recommendations for future work.

II. Background

2.1 Airmass Thunderstorm Development

Airmass thunderstorms are isolated cumulonimbus clouds that develop due to localized convection in an unstable airmass (Wallace and Hobbs 2006). These storms are also referred to as single-cell or pulse thunderstorms, due to a characteristic small and centralized area of enhanced precipitation. The development of airmass thunderstorms is most common during the summer months in Florida, but can happen throughout the year. Since these storms are the result of local convection, they differ from thunderstorms that form along fronts, instability lines, or upper level troughs, which are typically multicellular, more vigorous, and longer lasting. Thunderstorms due to frontal systems are most common during the late fall to early spring seasons in Florida.

Airmass thunderstorms require three basic ingredients to form: moisture, instability, and lift. In Florida, abundant moisture is provided by the Atlantic Ocean to the east and Gulf of Mexico to the west. Instability exists due to Florida's sub-tropical latitude and coincident strong solar heating. Lift is the most complex and variable of the three ingredients. Over KSC/CCAFS/PAFB, lift exists as complicated interactions between localized circulations, such as sea, river, and lake breezes, which are most vigorous during the summer months. Other local low-level boundaries include horizontal convective rolls, frictional convergence lines, and lake shadow lines (Roeder 2015). Preexisting thunderstorms can also produce outflow boundaries that can serve as lifting mechanisms for future storms.

The sea breeze, onshore flow caused by differential heating between the land and ocean, creates a sea breeze front over KSC/CCAFS/PAFB. This localized front acts as a focal point for airmass thunderstorms. Additionally, the Banana and Indian

Rivers, which surround KSC, also cause localized circulations referred to as river breezes. There are also numerous lakes in the region that produce minor localized circulations. At low levels, many of these local circulations converge with one another, serving as trigger points for lift and convection over the areas 45 WS supports, as shown in Figure 1. Under some flow regimes, even the sea breeze front that forms in Western Florida along the Gulf of Mexico can travel eastward across the state, creating additional areas of convergence.

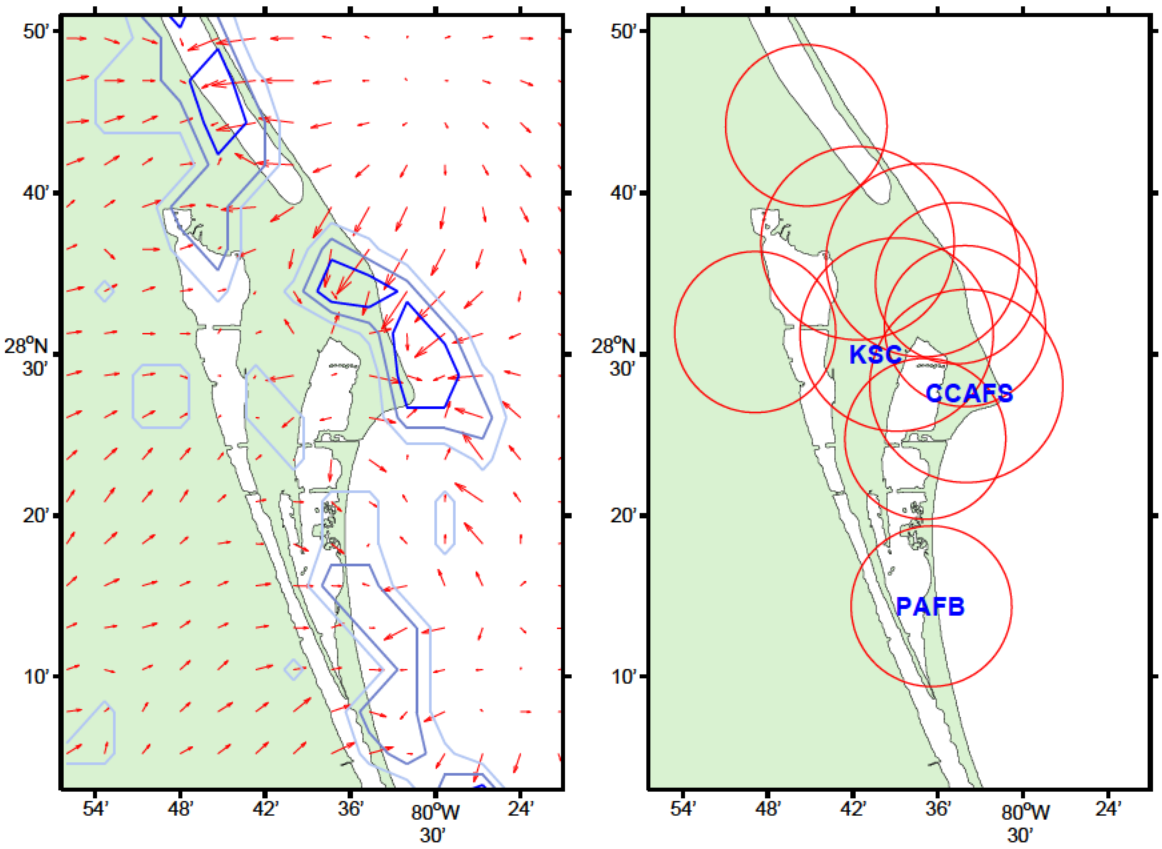

Figure 1. The left image displays a typical sea breeze setup along the East-Central Florida coast. Using a 5 km NAM forecast valid 1800 UTC 22 Jun 2014, 1000 mb wind vectors are displayed in red with areas of convergence outlined in blue. The darkest contours outline areas of maximum convergence. Low-level convergence acts as a lifting mechanism that triggers airmass thunderstorms over KSC/CCAFS/PAFB (locations displayed to right). The right image also outlines the 5 and 6 nm warning circles 45 WS provides coverage for. Right image adapted from (Roeder et al. 2014).

Airmass thunderstorms were studied in significant detail as part of the Thunderstorm Project during the late 1940s (Byers and Braham Jr. 1948). This project pioneered the understanding of thunderstorm development, and its basic concepts are still valid today. The study examined Florida and Ohio thunderstorms through use of ground instruments, weather balloons, and flying P-61 aircraft through designated levels of a thunderstorm (Byers and Braham Jr. 1948). The study broke the life cycle of a thunderstorm into three stages of development: the cumulus stage, the mature stage, and the dissipating or anvil stage.

The cumulus stage of development consists of an updraft that lifts warm moist air, causing a cumulus cloud to form and expand. The cloud growth occurs as rising air expands and cools adiabatically, resulting in water vapor condensing on cloud condensation nuclei. The updraft speed increases with height inside the cloud and entrainment occurs as air outside the cloud flows into the lateral edges of the developing cumulus (Wallace and Hobbs 2006). The strong updraft, normally around $10\,\mathrm{m\,s^{-1}}$, can result in supercooled droplets existing above the freezing level and mixing with frozen hydrometeors. The term supercooled droplets refers to cloud droplets that exist as a liquid below a temperature of 0°C in the absence of sufficient nucleation sites. The cumulus stage has a typical duration of 10–15 min (Rogers and Yau 1989).

The mature stage begins when rain droplets, formed by collisions and coalescence of smaller cloud droplets within the updraft, start to fall as precipitation. The falling droplets drag air particles downward, causing a downdraft to form (Wallace and Hobbs 2006). The downdraft is also enhanced by evaporational cooling of rain droplets below the cloud base. Downdrafts reach the surface as a core of cold air where precipitation is occurring, altering the surface wind flow and initial buoyancy characteristics that were present during the cumulus stage (Rogers and Yau 1989). The top of the cloud cell extends to at least 25 000–30 000 ft during the mature stage

and consists of liquid cloud and rain droplets, snowflakes, ice crystals, and graupel (Byers and Braham Jr. 1948). Graupel is a rimed ice particle formed by the accretion of supercooled cloud droplets on an ice crystal. Frozen hydrometeors, such as graupel, can exist in a frozen state at temperatures above 0°C as they slowly melt while descending in the downdraft, while supercooled droplets continue to exist in the remaining updraft regions. The interactions between these mixed phase hydrometeors create areas within the cloud where charging occurs, and are important regions to identify when predicting lightning initiation.

The mature stage typically lasts 15–30 min before giving way to the dissipating stage (Rogers and Yau 1989). A storm dissipates as the downdraft circulation expands and envelopes the entire cloud, cutting off the remaining updrafts (Wallace and Hobbs 2006). Without fuel from the updraft, the cumulus cell rains itself out and begins to decay. This decay process can only be avoided if enough vertical wind shear aloft exists to direct any lingering updrafts away from the precipitation induced downdraft. However, within a typical airmass thunderstorm over Florida, the vertical wind shear is generally very weak or non-existent. An airmass thunderstorm without sufficient vertical shear to maintain the updraft has a complete lifetime of 55–75 min (Rogers and Yau 1989). The three stages of airmass thunderstorms development, including the associated updraft and downdraft motions, are depicted in Figure 2.

2.2 Cloud Electrification

The electrification of a developing airmass thunderstorm occurs due to a combination of several processes. Ion capture mechanisms, inductive charging of rebounding particles, non-inductive charging, and convection methods have all been studied and hypothesized to contribute to electrification in the atmosphere (MacGorman and Rust 1998). However, most of those processes are too slow to support electrification over

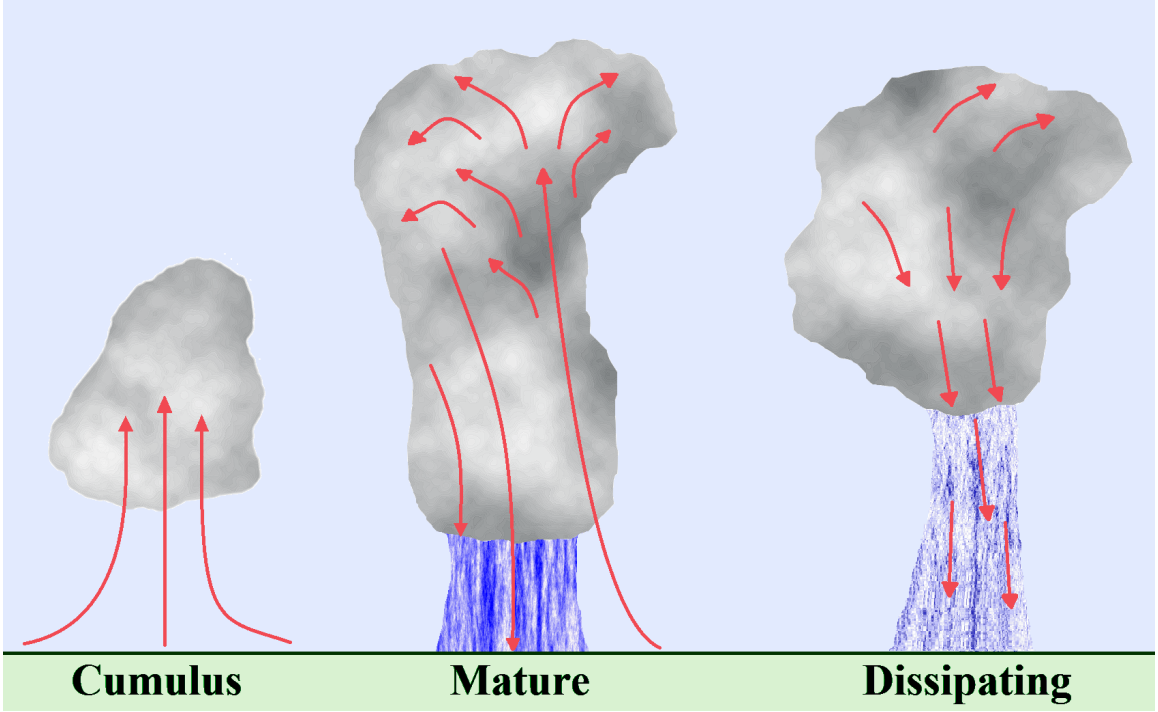

Figure 2. A graphical depiction of the three stages of airmass thunderstorm development. The red arrows represent the general flow associated with each stage of development. Image adapted from (Byers and Braham Jr. 1948).

the relatively short duration of an airmass thunderstorm. Of the four methods mentioned, the only one that supports the rapid buildup of charge and is examined in this study is the non-inductive charging mechanism.

Non-inductive charging resulting from the graupel-ice mechanism is generally accepted as the dominant electrification process in thunderstorms (Wallace and Hobbs 2006). Non-inductive implies that the hydrometeors involved are not required to be polarized by the ambient electric field. The graupel-ice mechanism produces charges through collisions between falling graupel and stationary to upward moving ice crystals that make up portions of the cloud (MacGorman and Rust 1998). This interaction occurs as small, light ice crystals ascend with the updraft, while graupel gains mass through accretion and descends once it becomes too heavy for the updraft to support. Supercooled water droplets must also be present during the charging process as they

have been experimentally shown to facilitate significant charge transfer (Reynolds et al. 1957).

The collisions between graupel and ice create a main charging zone, consisting of a net negative charge between the $-10°C$ and $-20°C$ temperature levels in the cloud (Rakov and Uman 2003), with a mean height of $-15°C$ (Reynolds et al. 1957). Experiments to determine exactly where this negative charge region occurs have found that it depends on a number of factors, including ice crystal dimension, particle relative velocity, liquid water content, and chemical impurities (Jayaratne et al. 1983). The negative charge zone around $-15°C$, combined with net positive charges in the upper and lower regions of the storm, creates a vertical tripole structure in the charge distribution within an airmass thunderstorm. The positive charges in the upper region are caused by an upward flux of charged ice crystals, and the lower region charge is caused by falling graupel that is positively charged (Wallace and Hobbs 2006).

2.3 Lightning Discharge

Lightning occurs when the electric fields created by a developing thunderstorm exceed approximately $3 \times 10^6\,\mathrm{V\,m^{-1}}$ (Rakov and Uman 2003). This is the field strength required for the dielectric breakdown of cloudy air at altitudes near 6 km, but it can vary depending on factors such as altitude and the presence of hydrometeors. Aircraft measurements have shown that large scale electric fields within a thunderstorm are typically near $3 \times 10^5\,\mathrm{V\,m^{-1}}$ (MacGorman and Rust 1998), which are too weak to cause the initial dielectric breakdown of the air. This discrepancy has led researchers to suggest that lightning initiates as a result of emission of positive corona from the surface of precipitation particles, causing the electric field to become locally enhanced and supporting the propagation of a corona streamer (Rakov and Uman 2003).

A lightning flash consists of that initial breakdown, followed by a stepped leader.

Stepped leaders lower charge from the cloud to the location of lightning termination. Each leader has a typical length of 50 m and duration of 20–50 µs (Rakov and Uman 2003). The leader then connects to a grounded object during the attachment process. The grounded object can either be the ground itself or a region of opposing charge aloft. The attachment process is followed by the return stroke. A return stroke is the most luminous lightning process and is a flow of current through an ionized channel between the cloud and the lightning termination point (Rakov and Uman 2003). A lightning discharge often consists of an initial return stroke followed by several subsequent return strokes. The initial return stroke typically propagates at $^1/_3$ to $^2/_3$ the speed of light. Any subsequent strokes are usually initiated by dart leaders, which are similar to stepped leaders, except they follow the path initially created by the return stroke.

2.4 Lightning Detection

Due to the sensitivity of operations at KSC/CCAFS/PAFB, a vast network of lightning and electric field monitoring instruments is installed. There are four major systems, which when used in conjunction, provide a near 100% detection rate of lightning in and around the location of the sensors (Roeder 2010). The principle lightning detection system used by 45 WS is the Four Dimensional Lightning Surveillance System (4DLSS). This system detects lightning aloft using the Lightning Detection and Ranging System (LDAR), and CG lightning using the Cloud-to-Ground Lightning Surveillance System (CGLSS). The two other systems frequently utilized are the NLDN and a locally developed Launch Pad Lightning Warning System (LPLWS).

2.4.1 LDAR

LDAR detects lightning aloft, which includes cloud-to-cloud (CC), intra-cloud (IC), and cloud-to-air (CA) lightning. It can also detect CG lightning, but is unable to accurately depict the location of a ground strike. LDAR was developed by NASA scientists in the mid 1970s to assist with lightning research at KSC. The first LDAR became operational in the early 1990s (Starr et al. 1993), and quickly became an essential tool for lightning detection and advisory issuance. The original system, LDAR-I, consisted of seven VHF radio receivers with a 66 MHz center frequency and 6 MHz bandwidth. The network consisted of a central receiver at KSC surrounded by six additional receivers spaced approximately 10 km apart. Due to the high cost and difficulty to maintain the aging LDAR-I sensors and central processor, it was replaced by LDAR-II (Roeder 2010). The installation of the new system began in 2006, and it became operational and started archiving data in 2008.

LDAR-II operates using the same receiver frequencies as LDAR-I, though the system now consists of nine receivers spread throughout KSC, CCAFS, and other nearby areas. The system uses a time-of-arrival method to determine the time, X (east/west), Y (north/south), and Z (altitude) coordinates of an electromagnetic (EM) discharge from a stepped leader. When a stepped leader occurs, the time of the resulting EM pulse is recorded by each receiver, and a hyperbolic volume solution between pairs of receivers is calculated (Roeder 2010). A three dimensional location of the stepped leader is then determined by the intersection of four different hyperbolae solutions. Due to the short duration of the stepped leaders, LDAR-II requires timing precision to a millionth of a second, and the system must automatically perform a time calibration event every four seconds. For visual reference, two and three dimensional images of LDAR-II data are displayed in Appendix A. Additionally, since LDAR-II is the current system in operation, subsequent references will refer to it as LDAR.

2.4.2 CGLSS

CGLSS is used to detect the polarity and impact location of CG lightning. The original system was installed during the summer of 1979, but has been upgraded several times over the years, and is now referred to as CGLSS-II (Mata and Wilson 2012). CGLSS-II currently consists of six sensors, but the sensors are no longer manufactured and limited replacement parts exist. Therefore, any future sensor degradation will likely require replacement of the entire system in the next few years (Roeder 2012). With a six sensor configuration, CGLSS-II has a CG lightning detection rate near the launch pads of 96% with strike location accuracy of 330 m. Further references to the CGLSS-II system will use the term CGLSS.

CGLSS utilizes magnetic direction finding and time-of-arrival methods to resolve the location of a return stroke (Roeder 2010). Each sensor consists of two wire-loop antennas that detect currents induced by magnetic fields associated with a return stroke. The current generated in the loops is related to the magnetic field strength of the return stroke by the cosine of the angle between a loop antenna and the direction of the lightning strike. The direction of the flash can then be determined by comparing voltages generated in each antenna loop (Cummins et al. 1998). At least two sensors are required to determine a location using magnetic direction finding (Roeder 2010). Using the time-of-arrival method, three or more pairs of sensors are used to determine lightning position in a similar fashion as LDAR, with the exception that CGLSS is optimized to detect EM frequencies associated with return strokes. All six CGLSS sensors in combination provide multiple solutions for each detection method, so a single optimized ground location is calculated based on a statistical chi-squared minimization (Roeder 2010).

CGLSS can detect multiple return strokes in real-time, which allows 45 WS to pinpoint exactly where strokes impact the ground and what facilities may have been

struck. Rakov and Uman (2003) state that the current associated with a return stroke likely results in the most damage caused by a lightning strike. When CG lightning occurs, CGLSS provides an advantage over LDAR , which loses detection efficiency below an altitude of 1.0 km (Roeder et al. 2005). CG lightning strike locations are compiled daily by 45 WS and reported to operators and facility managers. This is to ensure that proper testing is completed on sensitive payload and launch vehicle electronics that are within a specific proximity of CG lightning strikes (Roeder et al. 2005). A map of the 4DLSS sensors, which includes LDAR and CGLSS, are depicted in Figure 3.

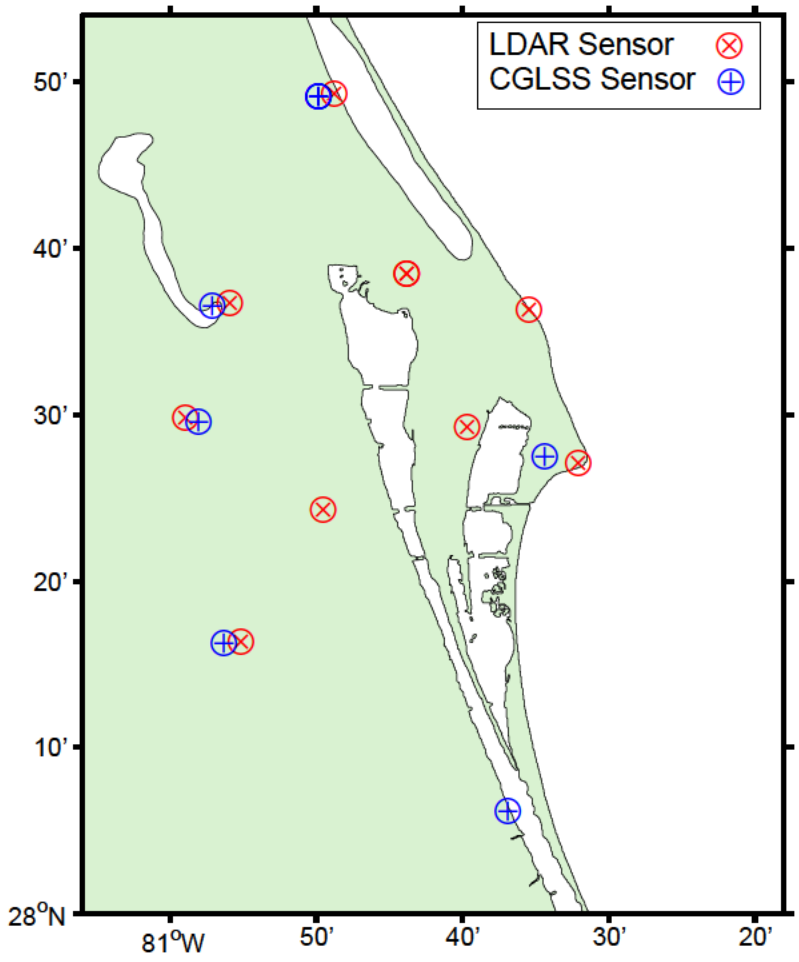

Figure 3. Locations of the 4DLSS sensor network. The three westernmost CGLSS sensors are located within 300 m of LDAR sensors.

2.4.3 NLDN

The NLDN is a commercial lightning detection system operated by Vaisala. It consists of more than 110 remote sensors across the United States, including one just north of PAFB (Vaisala 2013). The network operates using principles and equipment analogous to CGLSS. Each NLDN sensor detects EM signals associated with return strokes and uses magnetic range finding and time-of-arrival information to determine the time, location, polarity, and amplitude of CG lightning. The NLDN can also detect lightning aloft, but it has a significantly lower detection efficiency than LDAR. Due to sensor spacing differences and detection range requirements of the NLDN and CGLSS, each system can lose detection efficiency based on the intensity of a return stroke. The NLDN loses detection efficiency for weak return stokes near KSC/CCAFS with a peak current below 7 kA, which CGLSS can detect (Roeder 2010). Conversely, CGLSS can fail to detect strong local return strokes with peak currents above 50 kA, which the NLDN can detect. Therefore, using the two systems in conjunction ensures maximum CG lightning detection efficiency for 45 WS.

2.4.4 LPLWS

The LPLWS is a network of 31 electronic field mill sensors spread across KSC and CCAFS. Each field mill measures the surface electric potential, and uses that information to generate and display electric field contours in $\mathrm{kV\,m^{-1}}$ based on one minute averages (Eastern Range Instrumentation Handbook 2003). When a thunderstorm or developing convective cell moves toward a field mill, the charge within the cloud will cause significant changes to the ambient electric field measured at the sensor. The induced charge can either become strongly negative or positive, depending on the type of cloud and its corresponding charge distribution.

Murray et al. (2005), Beasley et al. (2008), and da Silva Ferro et al. (2011) conducted studies relating lightning onset to electric field mill readings, but encountered mixed results. Overall, it was found that measured changes in the ambient electric field were limited in trying to predict exactly where and when a lightning strike would occur. Despite this limitation, LPLWS is a key component of the lightning launch commit criteria (LLCC) that 45 WS must evaluate during a launch process. The LLCC are a set of 12 rules developed to avoid triggered and natural lightning (Roeder and McNamara 2006). Since rocket triggered lightning can occur when there are no thunderstorms present, electric field data is a useful tool for assessing the risk. Surface electric fields with absolute values over $1.0\,\mathrm{kV\,m^{-1}}$ cause delays when convective clouds are present. Values over $1.5\,\mathrm{kV\,m^{-1}}$ within 5 nm of the flight path will delay launches by at least 15 min, independent of what cloud types are present.

2.5 Weather Radar

Two weather radars provide coverage of the 45 WS forecast area. One is the WSR-88D at KMLB, operated by the National Weather Service (NWS), and about 50 km south of KSC. The other is a Radtec Titan C-Band Doppler Radar with a 4.3 m antenna and 250 kW average transmission power (TDR 43-250). This radar was installed in 2009, replacing the WSR-74 at PAFB (Roeder et al. 2009). The TDR 43-250 is controlled locally by 45 WS, and is installed 43 km southwest of the KSC/CCAFS launch pads. This location is optimized for evaluation of radar signatures related to the LLCC and to track the local sea and river breeze fronts. The TDR 43-250 does provide DP capability, but due to a lack of archived data and limited performance testing, the TDR 43-250 was not used in this study, and will not be discussed in further detail. A map displaying the the locations of the KMLB WSR-88D and the TDR 43-250 is shown in Figure 4.

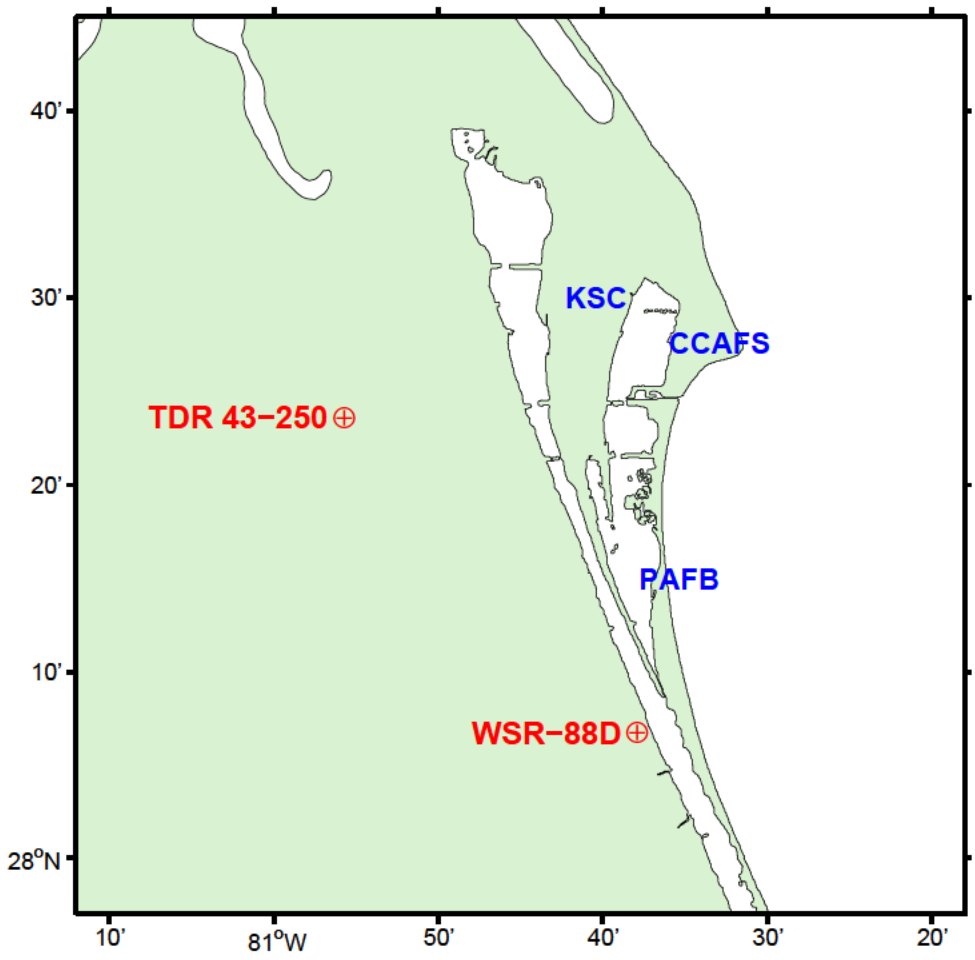

Figure 4. Locations of the two weather radars in East-Central Florida utilized by 45 WS forecasters. The general locations of installations 45 WS supports are also shown.

2.5.1 WSR-88D

The WSR-88D at KMLB is one of 160 installed across the United States and select locations overseas (NWS 2014). It is an S-Band Doppler radar with a 10 cm wavelength. The radar operates by transmitting EM pulses with an average power of 450 kW (NWS 2014). It then measures EM waves reflected by targets, such as raindrops, to determine intensity, location, and movement. The two main operating modes of the radar are clear air and precipitation. The radar is operated in clear air mode when precipitation is not expected, and it takes 10 min to complete a volume

scan. In precipitation mode, the radar completes an entire volume scan every 4–6 min depending on the specific volume coverage pattern (VCP) in operation. Precipitation mode VCPs are tailored based on precipitation type, and they provide more elevation slices than clear air mode VCPs. The WSR-88D has a maximum range of 230 km.

Before 2011, all WSR-88Ds only transmitted and received EM pulses with horizontal polarization (NWS 2014). As of 2014, over 150 sites had upgraded to DP, which transmits and receives backscattered EM pulses with both horizontal and vertical polarization. This allows the radar to estimate the horizontal and vertical dimensions of targets, providing improved size, shape, and diversity characteristics of hydrometeors. Those characteristics permit the ability to discriminate between types of hydrometeors, such as rain, snow, hail, and ice, as shown in Figure 5. Even though WSR-88Ds were only upgraded to DP capability over the past two to three years, the theory and applications of polarimetric weather radars has been studied extensively for over 30 years (Bringi and Chandrasekar 2001).

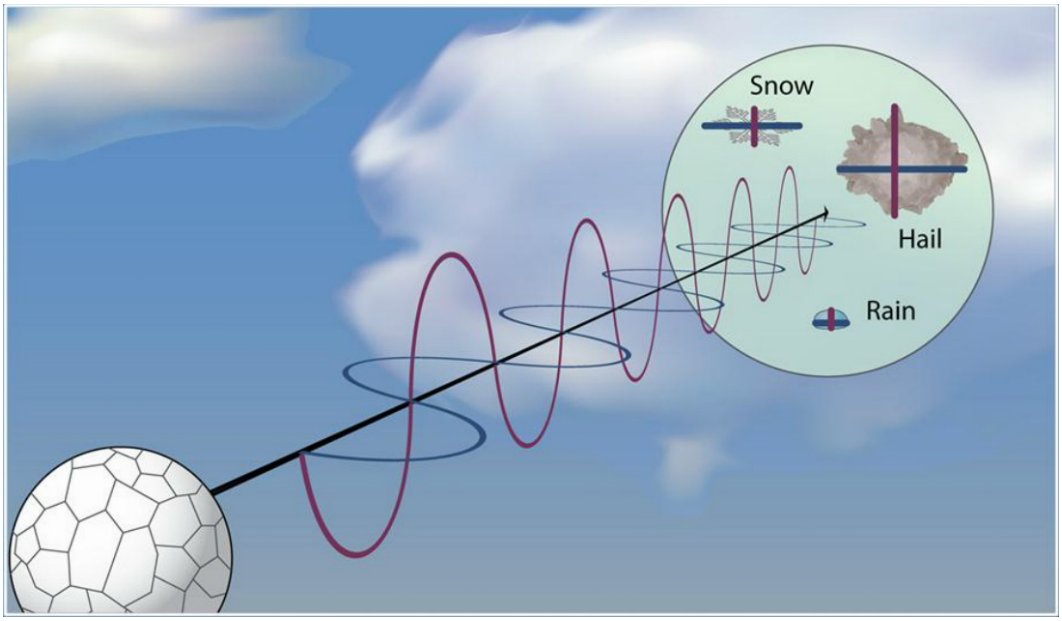

Figure 5. Illustration showing the vertically and horizontally polarized waves utilized by a DP weather radar. The backscatter from the two waves can provide information about the size and shape of a target. Public domain image courtesy of NWS (2014).

WSR-88D data is available to users through Level-II and Level-III datasets. Level-II is the base data at normal resolution and consists of reflectivity, spectrum width, and mean radial velocity measurements (NWS 2014). Base data is also used to produce derived products, which include vertically integrated liquid (VIL), storm total precipitation, and several DP products. Level-III data consists of 41 products that are available as digital images directly from the NWS. This format was developed to use less bandwidth and is therefore at a lower resolution than Level-II data.

2.5.2 Reflectivity

Radar reflectivity is the most heavily utilized WSR-88D product for short-term weather forecasting and lightning initiation studies. This is due to the direct correspondence between reflectivity and precipitation intensity. Reflectivity values are determined by first calculating the power the radar receives from a target volume (Rinehart 2010). Using the Rayleigh assumption, which applies since hydrometeors are typically much smaller than the radar's transmitted wavelength, the power equation is:

$$p_r = \frac{\pi^3 p_t g^2 \theta \phi c t |K|^2 l z}{1024 \ln(2) \lambda^2 r^2} \tag{1}$$

where p_t is the transmitted power, g is the gain, θ and ϕ are the horizontal and vertical beam widths, ct is the pulse duration (t) multiplied by the speed of light (c). K represents the complex portion of the index of refraction, l represents attenuation, z is the radar reflectivity factor, λ is the wavelength, and r is the distance from the radar (Rinehart 2010). For a given radar, including the WSR-88D, p_t, g, θ, ϕ, t, and λ are constant parameters. A specific value for K can also be specified assuming that the radar is primarily interested in interrogating liquid hydrometeros. Additionally, the attenuation is ignored, since it is often unknown. Grouping all the constants

together, the radar equation becomes:

$$p_r = \frac{c_2 z}{r^2} \tag{2}$$

where c_2 combines the constants above (Rinehart 2010). The equation can then be rearranged to solve for z:

$$z = c_2 p_r r^2 \tag{3}$$

which indicates that the radar reflectivity factor is proportional to the power received and the range squared. A final adjustment to this equation is made to account for the variation between the size of particles in a sample volume. The size can range from very small fog droplets at $0.001\,\mathrm{mm^6\,m^{-3}}$ to hail which can be as large as $36\,000\,000\,\mathrm{mm^6\,m^{-3}}$. To account for the huge range of values, a logarithmic radar reflectivity value of Z can be defined as:

$$Z = 10 \log_{10} \frac{z}{1\ mm^6\ m^{-3}} \tag{4}$$

where Z is in units of decibels (dB) relative to $1\,\mathrm{mm^6\,m^{-3}}$ (dBZ). The logarithmic adjustment results in a range of Z values from near $-30.0\,\mathrm{dBZ}$ for fog to $77.0\,\mathrm{dBZ}$ for large hail (Rinehart 2010). All preceding usage in this document of the terms "radar reflectivity" or simply "reflectivity" referred to Z.

2.5.3 Differential Reflectivity

Differential reflectivity (Z_{DR}) is a DP product that is calculated using the horizontal (z_H) and vertical polarization reflectivity factor (z_V):

$$Z_{DR} = 10 \log_{10} \frac{z_H}{z_V} \tag{5}$$

with Z_{DR} measured in dB (Rinehart 2010). Since Z_{DR} includes measures of the vertical and horizontal axis of a target, it is valuable in determining the shape of hydrometeors. Objects that are spherical will have nearly identical values of z_H and z_V, resulting in Z_{DR} values near 0.0 dB while non-spherical objects will either have positive or negative Z_{DR} values depending on the ratio of z_H to z_V. Z_{DR} can also be enhanced by increases in the complex refractive index. Water droplets, which have a higher complex refractive index than ice, have higher Z_{DR} than solid ice pellets of similar size and shape (Kumjian 2013a). When reflectivity is measured logarithmically using Z_H and Z_V, Z_{DR} is more simply defined as:

$$Z_{DR} = Z_H - Z_V \tag{6}$$

Z_{DR} can vary greatly for different types of hydrometeors. Large raindrops experience drag as they fall, causing them to flatten and spread out horizontally, increasing Z_{DR} relative to smaller drops, which do not experience as much drag and deformation (Kumjian 2013a). Since rainfall is typically heavier when larger drops are present, Z_{DR} can be used to determine rainfall intensity. Though Z_{DR} measurements are useful for rainfall estimates, they can vary dramatically when examining hail and graupel due to variable hailstone shapes and sizes. Most hailstones are spherical, producing Z_{DR} close to 0.0 dB. Very large hail can even produce negative Z_{DR} when the stones become large enough (≥ 5 cm in diameter) that complex resonance scattering effects become important (Kumjian 2013a). Despite the variation in Z_{DR} for hail, it can be useful for detecting large hail by comparing areas of high Z_H to areas of low Z_{DR}, and also by identifying where near 0.0 dB Z_{DR} values are embedded in areas of high Z_{DR} caused by heavy rain (Bringi et al. 1984).

Within a convective cell, a column of enhanced Z_{DR} values can exist above the freezing level in what is known as a Z_{DR} column. These columns of enhanced Z_{DR},

with values up to 3.0–4.0 dB, identify the location in convective updrafts where supercooled water droplets and wet ice particles are lofted to altitudes above the freezing level. Z_{DR} columns tend to exist within the updraft maximum of ordinary convective storms and along the periphery of the updraft maximum in supercells (Kumjian 2013b). Due to their presence in ordinary convective storms, Z_{DR} columns can be useful in identifying when a convective cell has the sufficiently strong updraft and mixed phase hydrometeors, such as graupel and supercooled water droplets, necessary to produce the charging required for lightning initiation. Z_{DR} columns can best be identified using a vertical radar cross section, which is shown in Figure 6.

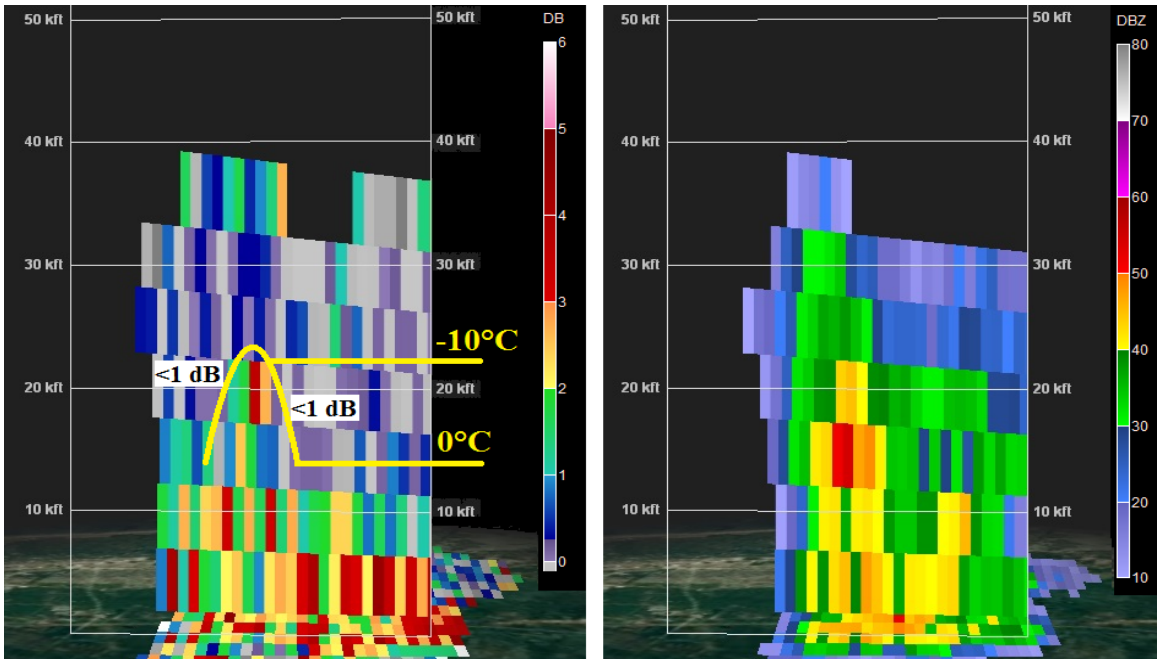

Figure 6. A radar cross-section with Z_{DR} on the left and Z on the right. A well defined column of $Z_{DR} \geq 1.0$ dB extends within the updraft core of this storm from the 0°C to −10°C heights.

2.5.4 Specific Differential Phase

Specific differential phase (K_{DP}) is a DP product that is calculated by examining the phase difference between the vertically and horizontally polarized radar signals

(Rinehart 2010). When EM radiation propagates through hydrometeors that are not perfect spheres, it results in a phase shift that varies between horizontal and vertical polarizations (Kumjian 2013a). This is known as differential phase (ϕ_{DP}), which is defined as:

$$\phi_{DP} = \phi_{HH} - \phi_{VV} \tag{7}$$

where the first subscripts of ϕ_{HH} and ϕ_{VV} each represent a phase shift between the received and transmitted energy due to attenuation by a target. Once ϕ_{DP} is calculated, K_{DP} can be defined as:

$$K_{DP} = \frac{\phi_{DP}(r_2) - \phi_{DP}(r_1)}{2(r_2 - r_1)} \tag{8}$$

with K_{DP} measured in $^\circ\,\mathrm{km}^{-1}$ (Rinehart 2010). By defining ϕ_{DP} in terms of half the range derivative, it provides a gradient of values along the radial direction, which can be more useful than examining ϕ_{DP} alone.

Positive K_{DP} is found in areas of rainfall, since falling raindrops are wider than they are tall, causing greater phase shifts along the horizontally polarized EM radiation (Kumjian 2013a). Therefore, K_{DP} can be useful to determine rainfall rates and total precipitation amounts. K_{DP} is not very useful for interrogating hail or snow, since they have K_{DP} values near $0.0\,^\circ\,\mathrm{km}^{-1}$ in most cases. However, for mixed phase hydrometeors, such as melting hail, the water shell around frozen ice can result in K_{DP} values of 6.0–$8.0\,^\circ\,\mathrm{km}^{-1}$. It has also been shown that strong electric fields in the ice regions of convective cells can align ice crystals horizontally or vertically, resulting in either negative or positive K_{DP} values aloft (Kumjian 2013a). This alignment is caused by strong electric fields near the top of a convective cloud and can be indicative of impending lightning.

2.5.5 Correlation Coefficient

Correlation coefficient (ρ_{HV}) is a DP parameter that measures the correlation between the horizontally and vertically polarized signal. It is defined as:

$$\rho_{HV} = \frac{(S^*_{VV} S_{HH})}{(|S_{HH}|^2)^{1/2}(|S_{VV}|^2)^{1/2}} \tag{9}$$

where S and S^* are the scattering matrices and the H and V subscripts represent the received and transmitted polarizations (Rinehart 2010). ρ_{HV} is useful in determining the diversity of scatterers in the radar sample volume. Regions dominated solely by rain will have ρ_{HV} at or just below 1.0, while frozen hydrometeors, which are more randomly orientated have ρ_{HV} values below 0.95, and as low as 0.80. This results in ρ_{HV} being useful for determining precipitation type.

2.6 Previous Research

2.6.1 Reflectivity and Lightning

Numerous studies have been conducted that relate Z to lightning initiation. Since the main charging zone within a cloud lies between the $-10°$C and $-20°$C thermal levels, previous studies focused on amplified Z values between those thermal levels, which is indicative of moderate levels of ice and graupel. Most prior studies have obtained results similar to the Pinder Principles. Buechler and Goodman (1990) analyzed 20 storms over Florida, New Mexico, and Alabama, and found a 1.0 probability of detection (POD) rate for lightning to occur when Z was at least 40.0 dBZ at the $-10°$C thermal level. This detection method resulted in lead times of 4–33 min before the first lightning flash occurred, with a false alarm ratio (FAR) of 0.20. That study utilized LDAR to detect lightning for several storms in the vicinity of KSC. The Buechler and Goodman (1990) results are very similar to those found by Dye

et al. (1989). In that study, aircraft, radar, and surface observations were used to examine cloud electrification in New Mexico. The research found that electric fields in a convective cell did not exceed 1.0 kV m^{-1} until Z exceeded 40.0 dBZ at the −10°C thermal level.

The significance of 40.0 dBZ at −10°C preceding lightning initiation was also confirmed by numerous other studies including Wolf (2006), Gremillion and Orville (1999), Vincent et al. (2003), and Yang and King (2010). Wolf (2006) was one of the largest studies as it examined over 1160 convective cells across the Southern United States from 2001–2006. Wolf showed that 40.0 dBZ at an updraft temperature of −10°C preceded CG lightning initiation with a POD of 0.96 and a FAR of 0.11. The updraft temperature was calculated by lifting a parcel from the surface and determining how high the −10°C level would be within a theoretical thunderstorm. This level will typically be several hundred to several thousand feet higher than the environmental −10°C level. Yang and King (2010) also had a larger sample size than many of the other studies, with 143 thunderstorms analyzed over Southern Ontario. This study tested thermal levels from −10°C to −20°C and Z values from 30.0–40.0 dBZ to determine which criteria produced the best results in predicting CG lightning onset in airmass thunderstorms. Much like the other studies, Yang and King (2010) concluded that 40.0 dBZ at the −10°C level gave the best POD, FAR, and critical success index (CSI) when predicting CG lightning onset, with an average lead time of 17 min.

Although most studies found the best statistical results with Z of 40.0 dBZ at −10°C, other studies, including Mosier et al. (2011) and Michimoto (1991) experienced their best results with different thresholds. Mosier et al. (2011) analyzed 67 384 convective cells over the Houston, Texas region and found that Z of 30.0 dBZ at the −15°C or −20°C level were the best predictors of CG lightning based on CSI statis-

tics. However, it should be noted that many of these studies utilized CG lightning, which often occurs after IC or CC lightning. Forbes (1993) found that LDAR detected lightning aloft an average of 5.26 min before the occurrence of CG lightning. That study also described several instances when weaker convective cells produced lightning aloft, but never produced any CG lightning. These weaker thunderstorms that do not produce CG lightning are the main reason why the Pinder Principles require a lower Z threshold for lightning aloft compared to CG lightning.

2.6.2 DP Parameters and Lightning

Since DP radar parameters provide additional details about the composition and structure of a convective cell, it can be a useful tool for recognizing the conditions required for lightning initiation. Hall et al. (1984) did some of the earliest work on identifying hydrometeor type based on Z and Z_{DR}. That research showed that rain, ice, and hail could be differentiated by correlations between Z and Z_{DR} in a particular radar echo. The study also recognized the presence of a column of elevated Z_{DR} values building around the 0°C level, indicating small supercooled water droplets being pulled into an updraft.

Illingworth et al. (1987) conducted some of the earliest examinations of Z_{DR} columns and found them to be associated with the developing stages of cumulus convection. Bringi et al. (1997) studied a multi-cellular thunderstorm over Florida, and encountered Z_{DR} columns that were coincident with the growth phases of each convective cell. These columns had maximum Z_{DR} values of 2.0–3.0 dB extending from the 0°C level that were capped off around −10°C. Inside a particular cell, the first IC lightning occurred within 6 min of mixed-phased conditions developing aloft, which also coincided with the fading of the Z_{DR} column. Carey and Rutledge (2000) closely examined lightning-producing storms in the tropics and developed methods

to identify when cloud electrification was occurring based on Z, Z_{DR}, and K_{DP}.

Since the 2012 upgrade of the WSR-88D to DP capability, two recent studies have utilized DP to predict lightning initiation and improve on methods that solely utilize Z. Woodard (2011) and Woodard et al. (2012) utilized a C-band DP radar in Alabama to determine if Z_{DR} in combination with Z led to statistical improvements in both CG and IC lightning prediction. This study examined 31 thunderstorm and 19 non-thunderstorm cases and found 40.0 dBZ at -10°C with Z_{DR} of at least 1.0 dB improved lead times by 30 s over a standard method of using 40.0 dBZ at -10°C. POD was slightly lower when using Z_{DR}, but FAR was also lower, causing a slight increase in overall CSI. Overall, the use of Z_{DR} did not produce statistically meaningful improvements in skill scores or lead times for the 50 storm sample size.

Woodard (2011) also incorporated particle identification (PID) into her study to directly test when graupel, hail, or supercooled water droplets were being observed by the radar. PID algorithms use fuzzy logic and DP parameters to determine the probabilities of specific hydrometeor types existing within a radar volume. The PID testing showed some promising results, particularly when the PID algorithm identified graupel at -15°C, but PID predicitors were not developed in this study due to the uncertainty and assumptions inherent with PID algorithms. The KMLB WSR-88D data does have the ability to view hydrometeor type using a hydrometeor classification algorithm (HCA), but it is only available for the three lowest volume scans. These lower scans fall well below the height of the thermal levels examined in this study for thunderstorms within 100 km of KSC, preventing the inclusion of HCA data.

Thurmond (2014) built upon the Woodard (2011) study by examining 68 convective cells over the KSC/CCAFS area during the summer months of 2012 and 2013. This research utilized the KMLB WSR-88D and CG lightning data to determine if the use of DP data could improve lightning initiation forecasts beyond what the Z

of 40.0 dBZ at −10°C method provides. In addition to testing methods using Z_{DR}, Thurmond (2014) also included K_{DP} in the study. The results showed that K_{DP} provided no added benefit, but the inclusion of Z_{DR} did lead to statistical improvements. The study analyzed Z values of 25.0, 30.0, 35.0, and 40.0 dBZ along with thermal levels of −10°C and −15°C. Z_{DR} values of 0.5, 1.0, and 1.5 dB were examined in conjunction with the above Z values and thermal levels. The best statistical results this study achieved, with an improved forecast lead time, occurred with $Z \geq 30.0$ dBZ at −10°C combined with $Z_{DR} \geq 0.5$ dB. These combined thresholds achieved an average lightning initiation forecast lead time of just under 19.5 min, which bested all methods using just Z at a specific thermal level by at least 3 min. This method also achieved a perfect POD of 1.0 and a FAR of 0.24.

III. Methodology

3.1 Convective Cell Selection

An initial database of 284 days with discrete convective cells was collected for a two year period ranging from March 2012–March 2014. Beginning with March 2012 provided two full years of WSR-88D DP radar availability, and allowed for analysis of both summer and winter season convection. Data was not collected from 6 December 2012–30 January 2013 due to a KMLB radar outage caused by construction of a taller radar tower needed to avoid beam blockage by new aircraft hangers built at KMLB. The initial database was built using composite WSR-88D Z data, archived every half hour at Plymouth State University (Plymouth State Weather Center 2014). Starting on 1 March 2012, when a discrete convective cell was observed, the date and time period of observation were recorded. An example of a day selected for further analysis is shown in Figure 7.

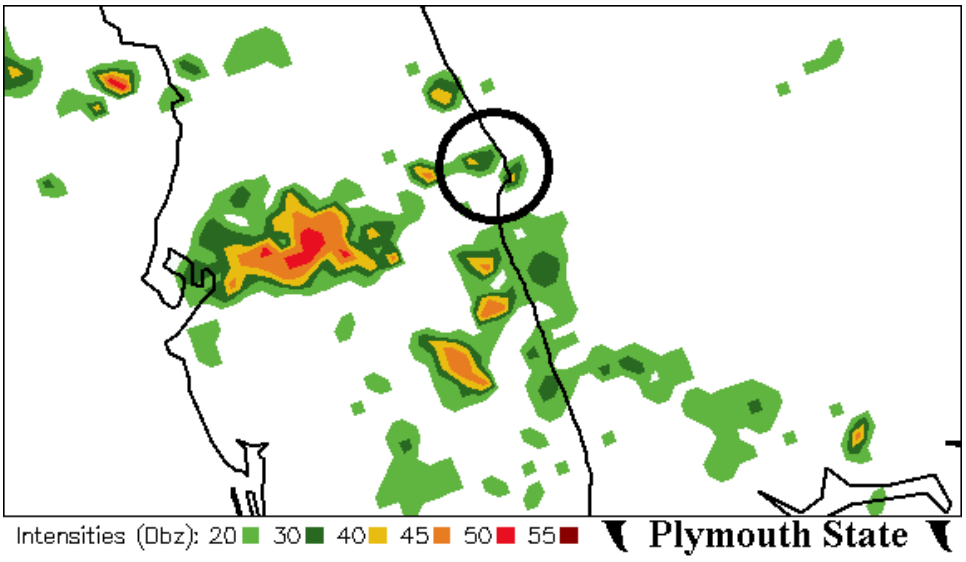

Figure 7. An archived composite reflectivity image showing several convective cells in Eastern Florida with a black circle outlining the location of Cape Canaveral. This day was chosen for further analysis to determine if it could be included in the training dataset. Image retrieved from Plymouth State Weather Center (2014).

Specific size and intensity criteria were not set when compiling the initial database. Instead, discrete convective cells were subjectively selected when they appeared significant enough to produce lightning based on size and composite Z alone. Since the focus was airmass thunderstorms, any days with complex areas or lines of thunderstorms related to synoptic scale frontal systems were omitted from the database. This was due to the difficultly in relating lightning initiation times to a specific convective cell within a larger complex of thunderstorms. Additionally, these types of thunderstorms are generally easier for 45 WS to forecast as it simply requires using weather radar and satellite data to time the approach of the frontal boundary.

Any days with tropical cyclone activity in the region were also omitted since thunderstorms associated with tropical cyclones are normally banded in nature with limited discrete cells. Additionally, the environment near a tropical cyclone will differ from that on a standard summer day in Florida. National Hurricane Center (NHC) past track seasonal maps from 2012, 2013, and 2014 (NHC 2014) were used to identify time periods with tropical activity within 500 km of KSC. On days without synoptic scale fronts or tropical activity, cells directly over the KSC/CCAFS/PAFB areas were preferred for further analysis, but any cells falling within 100 km of the central LDAR antenna at KSC were recorded. This distance allowed for a large number of convective cells to be included in the initial database, while minimizing any errors in LDAR location accuracy or detection efficiency, as shown in Figure 8.

3.2 Data

Archived 4DLSS data was downloaded from the Spaceport Weather Archive (KSC 2014). The archived data is organized by folder, with each containing one year of archives. Once downloaded, a yearly folder contains 12 folders for each month of the year. Each monthly folder contains over 1400 text documents organized chronologi-

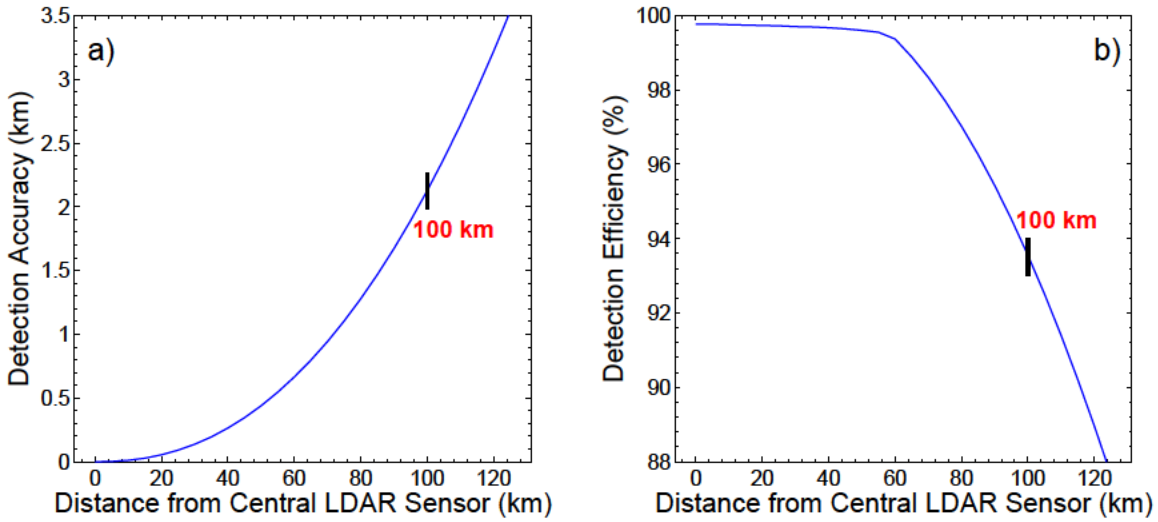

Figure 8. Accuracy and efficiency of the LDAR sensor network. Figure (a) shows detection accuracy is near 2 km at a distance of 100 km from the central LDAR sensor at KSC. Figure (b) shows detection efficiency is near 94% at a distance of 100 km. The two curves are approximations based on the current sensor configuration and are adapted from equations given by Murphy et al. (2008).

cally with files encompassing 30 min time periods. Each line of a given text document reports the event type (LDAR, CGLSS, or Calibration), Julian Day, time in UTC with precision to 1.0 µs, and the X, Y, Z coordinates of the event in meters relative to the central LDAR site at KSC. Each text document contains at least 900 lines due to calibration events, but some can contain over 500 000 lines when significant lightning activity is occurring within 200 km of KSC. There were a few time periods with missing data, but this had little impact on the research. The most significant data outage during the two year period of interest occurred from 21 December 2013–6 January 2014, which prevented one potential thunderstorm from being analyzed.

KMLB Level-II radar archives were downloaded from the National Climatic Data Center (NCDC) NEXRAD Inventory (NCDC 2014). Radar archives consist of gzip files for each time a complete radar scan occurs, which is typically every 4–6 min, depending on the VCP. Each file contains all available Level-II radar data at each elevation scan angle recorded for the given VCP. Radar archives were downloaded for

all 284 days with discrete convective cells, unless the radar was in a clear air mode VCP. If the radar was in clear air mode, that day was discarded from the initial database. For each day and time with discrete convective cells, radar archives were downloaded to encompass at least three hours before and three hours after the period of interest. This ensured that the entire life cycle of a target convective cell was contained within the archive, and not just the period of maximum intensity. Once days with radar outages, tropical activity, or periods with a clear air mode VCP were eliminated, 267 separate days of radar data were downloaded, with each day consisting of at least six hours worth of data. Additionally, there were seven days that consisted of separate morning and afternoon periods with discrete convective cells, bringing the total number of downloaded datasets to 274.

To identify the height of significant temperature levels in the atmosphere, rawinsonde observations were used. Rawinsondes are launched daily at the CCAFS Skid Strip (KXMR) at 0900 UTC. Additional launches also occur at times based on mission requirements, but are fairly infrequent. Since most lightning events occur during the afternoon in Florida, the 0900 UTC sounding occurs several hours before most convective development begins. However, under conditions when airmass thunderstorms occur, upper level temperature changes are minimal over periods of several hours. Additionally, the radial beam width of the radar at distances at which convective cells were interrogated causes a much greater source of error when trying to measure a specific thermal level compared to any minor errors caused by stale sounding data. Archived sounding data were obtained from the University of Wyoming Department of Atmospheric Science (Wyoming Weather Web 2014). If the KXMR sounding was not available, the Tampa Bay, Florida (KTBW) sounding was used. The KTBW rawinsonde is launched daily at 0000 and 1200 UTC, and was mainly utilized from 21 March 2013–8 May 2013 when KXMR data were not available.

3.3 Analysis

The database of 274 time periods with convective cells was split into training and validation datasets for analysis. The database was numbered 1 to 274 with the odd numbers becoming part of the training dataset. Since a majority of previous studies utilized CG lightning, it was necessary to create a training dataset to determine what critical Z and DP thresholds preceded all types of lightning. The database was originally ordered chronologically from March 2012–February 2014, ensuring that both the training and validation datasets had equal seasonal representation. This seasonal breakdown is displayed in Appendix B.

3.3.1 Training Dataset

The initial training dataset consisted of 137 time periods with archived radar data. For each time period, the most recent sounding was retrieved and heights of the $-5°$, $-10°$, $-15°$, and $-20°$C levels were recorded. These levels span the cloud charging zone where mixed phased hydrometeors are present. Each time period was then examined for discrete lightning or non-lightning producing convective cells that could be interrogated. Studies by Thurmond (2014) and Woodard (2011) both used the Larsen area method of radar analysis and lightning formation location (Larsen and Stansbury 1974) to determine which cells to investigate. Both studies defined their baseline for thunderstorm development as a Larsen area with $Z \geq 30.0$ dBZ above $-10°$C. In order to include a larger number of cells in this study, cells exceeding the height of the $-5°$C level were included. This selection method is similar to the lightning initiation study conducted by Hondl and Eilts (1994) over the KSC area in which any 10.0 dBZ radar echoes above the freezing level were used for analysis.

Once a cell was identified for further interrogation, it was analyzed to determine if the volume scan elevation angles of the KMLB radar intersected the cell at the

four thermal levels of interest. For most cells, the KMLB radar was set at a VCP that provided multiple elevation angles that properly intersected the four thermal levels. However, for some cells, a combination of the distance from the radar and the active scan elevation angles caused the radar to either miss the top of cells, or cause a single volume scan to contain multiple thermal levels of interest, as shown in Figure 9. When this occurred, the cell was rejected and not analyzed any further.

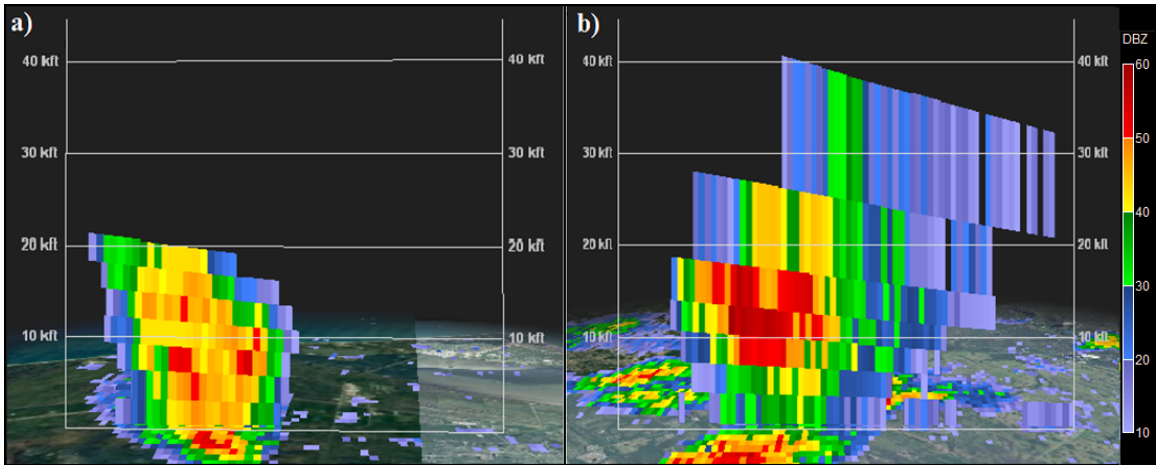

Figure 9. ***Z*** **cross-sections for two different cells rejected from the training dataset. In Figure (a), the scan elevation angle is not high enough to see** ***Z*** **values at or above the −10°C height, which was just above 20 000 ft. The VCP in Figure (b) has widely spaced scan elevation angles, resulting in volumes that span vertically by over 10 000 ft. These two examples were encountered several times when building the training and validation datasets.**

The remaining cells were then investigated to determine whether or not lightning occurred. Archived 4DLSS data was separated into LDAR and CGLSS strikes and plotted on a map of Florida. An archived radar image was also added to the map with the 4DLSS data overlaid to determine exactly when and where the initial flashes occurred from a cell of interest. If lightning occurred within a cell, the time of first 4DLSS report was recorded to the nearest second. If lightning did not occur, the cell was labeled as a non-lightning producing cell. Both lightning and non-lightning producing cells needed to be isolated enough from other cells in the area to confirm

whether or not lightning originated from a specific cell of interest. Typically, only one cell was analyzed on a given day, but several days had up to three lightning or non-producing cells that were analyzed. Images displaying good and poor examples of cells investigated in the training dataset are shown in Figures 10 and 11.

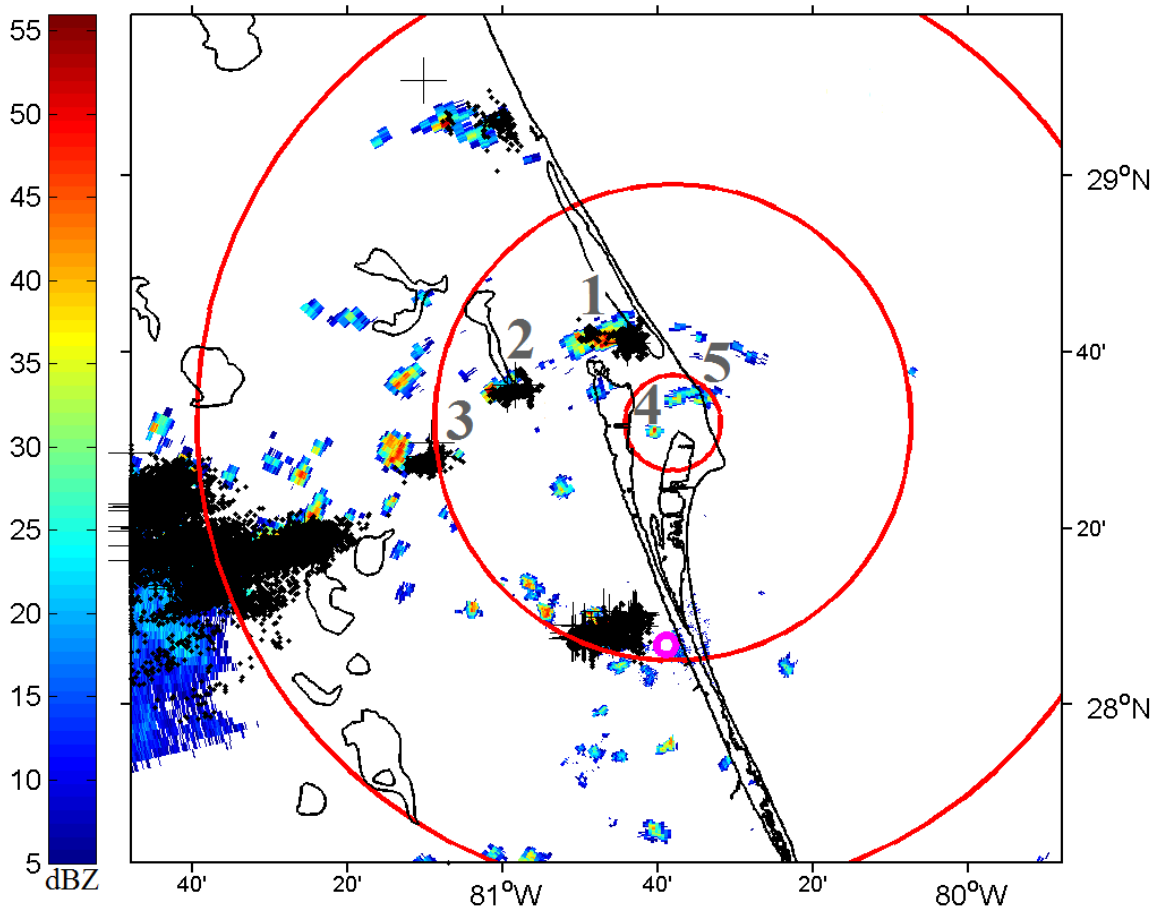

Figure 10. An example of a day with five ideal airmass type convective cells to analyze. This map contains a base radar reflectivity image with 4DLSS data overlaid. A black dot indicates an LDAR detection while a black plus indicates a CGLSS detection. The red circles represent distances 10, 50, and 100 km away from the central LDAR site, while the small magenta ring is centered on the KMLB WSR-88D. These circles were created as reference points to ease sorting through the 4DLSS archive for a particular lightning flash of interest. The three closest cells with lightning to the north and west of KSC/CCAFS are ideal lightning-producing cells for analysis while the two cells directly over KSC/CCAFS are ideal non-lightning producers. The lightning-producing cell 50 km south of KSC was not analyzed because it was too close to the radar to capture its vertical extent.

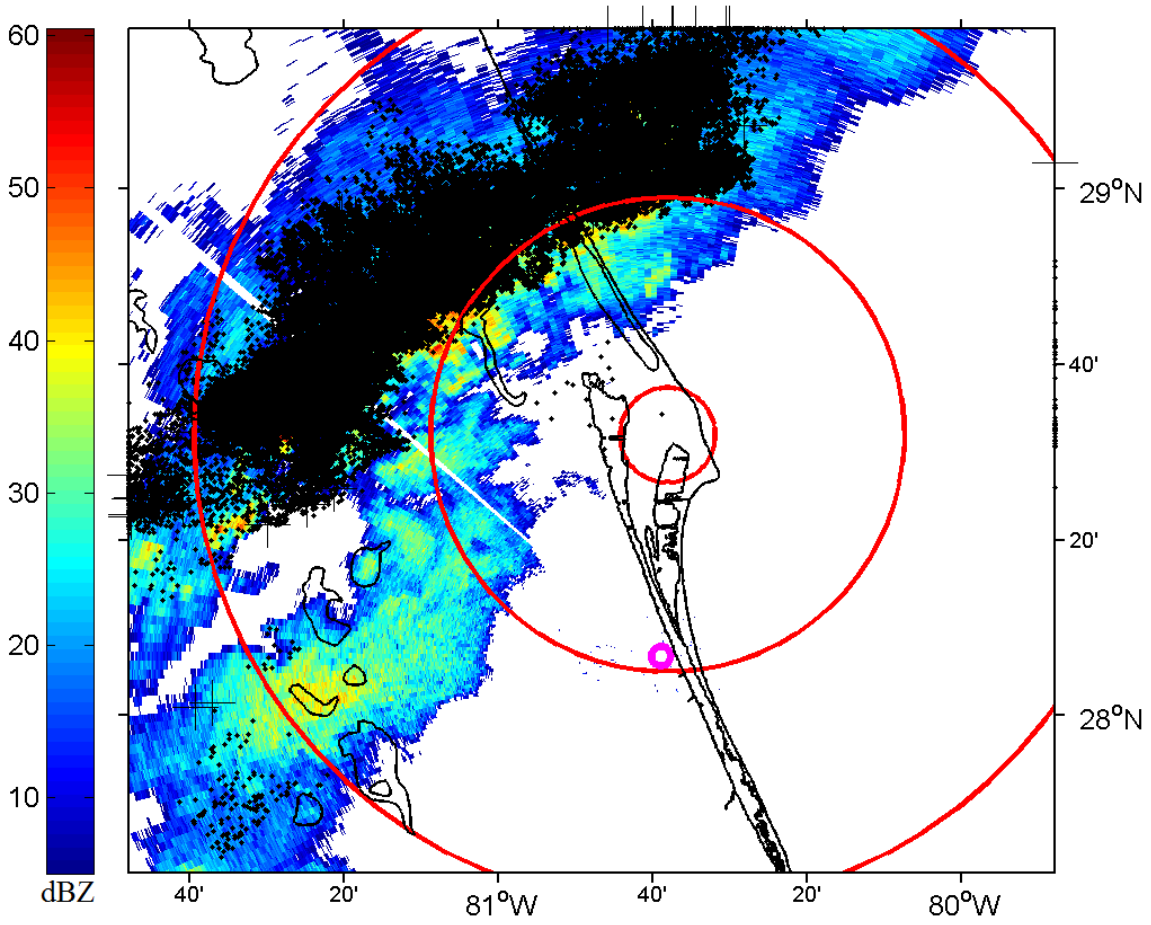

Figure 11. An example of a day without airmass type convective cells to analyze. This image displays a line of thunderstorms with a large cluster of 4DLSS detections across central Florida. This demonstrates the importance of having discrete cells as part of this research in order to determine when and where lightning occurred. This time period was rejected from the initial database of convective cells since the thunderstorms were not discrete in nature and likely caused by a frontal boundary.

Discrete convective cells became part of the training dataset when the VCP properly covered the thermal levels of interest, and archived 4DLSS data was available. For each lightning-producing cell, every volume scan up to 50 min before the occurrence of lightning was analyzed. For non-lightning producing cells, an artificial lightning occurrence time was set at when the cell achieved its maximum intensity based on peak vertical extent. Using GR2Analyst Version 2.13 software, Z, Z_{DR}, and K_{DP} were recorded at each thermal level of interest for every volume scan from 0–50 min

before the lightning initiation or peak intensity. The end time of each volume scan was also recorded, as well as the height of the top of the cell. The presence or absence of a Z_{DR} column was also noted for each cell. ρ_{HV} was briefly explored as a parameter to record, but was considered to be too indiscriminate to provide any useful data. An example of the displays used to perform this analysis with GR2Analyst is shown in Figure 12.

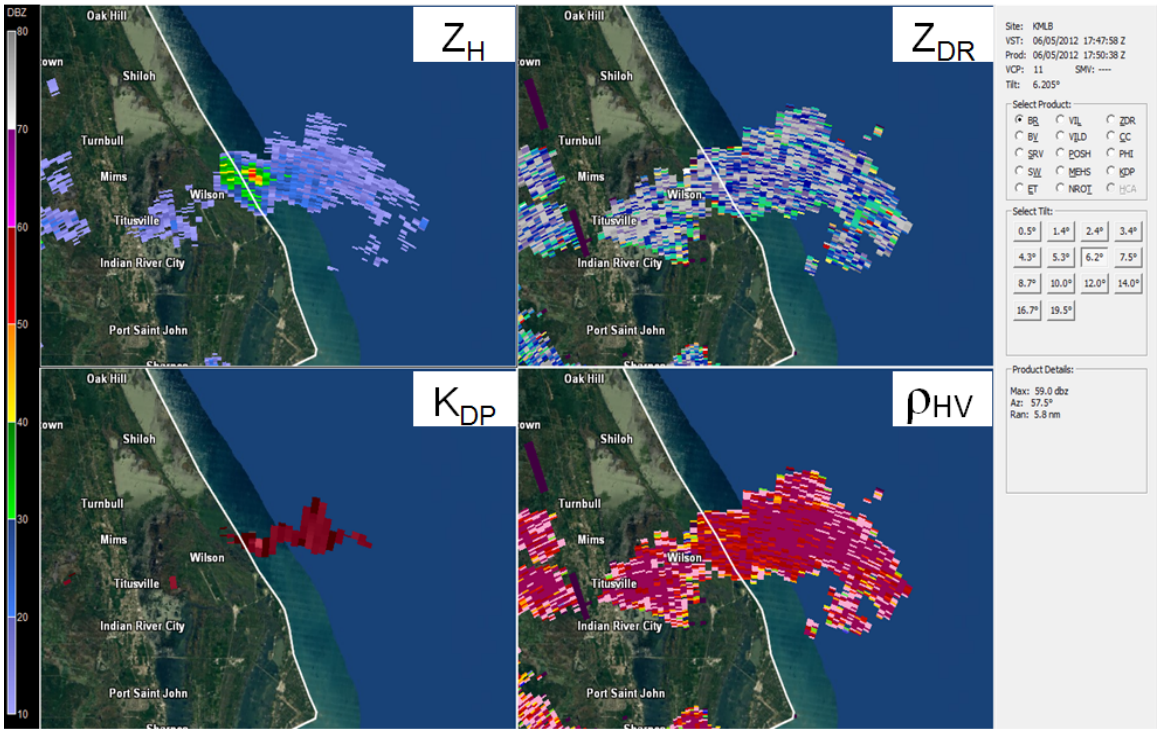

Figure 12. A four-panel GR2Analyst display with both Z and DP products used to analyze a cell over the northern part of CCAFS.

When analyzing a cell, each particular volume scan at one elevation angle can be several kilometers in height. The middle of an elevation scan was set as the actual height when determining whether or not a particular radar return was at or above a thermal level of interest. For each cell and time, the maximum Z was recorded when it occurred above one of the four thermal levels. The maximum Z_{DR} and K_{DP} values were then recorded within the updraft core that contained the maximum Z value.

The maximum Z, Z_{DR}, and K_{DP} would often occur in the same place, but Z_{DR} and K_{DP} were sometimes slightly displaced.

A total of 125 cells were analyzed in the training dataset with 74 producing lightning and 51 not producing lightning. All but one non-lightning producing cell exceeded the -10°C height. To determine optimal thresholds that could serve as test predictors for the validation dataset, cells in the training dataset were grouped by thermal level and whether they produced lightning. The data were also placed into 5 min blocks from 0–50 min leading up to lightning initiation for lightning-producing cells. For non-lightning producing cells, the data was binned into 5 min blocks leading up to when a cell achieved its maximum height. If there were two volume scans falling within a single 5 min time bin, the scan with the maximum Z value was placed into that bin.

Means, standard deviations, and t-scores were calculated to determine which time bins were statistically different from the overall mean at a particular thermal level. Scatter plots were also created to compare relationships between Z, Z_{DR}, and K_{DP}. Finally, signal detection models, as described in Jolliffe and Stephenson (2003), were examined to help determine which critical values maximized detection while limiting the number of false alarms. The analysis of the training dataset produced 18 different lightning predictors to compare with lightning aloft predictors from the Pinder Principles. The 18 predictors used either Z alone or a combination of Z and DP parameters at -5°C or -10°C.

3.3.2 Validation Dataset

The validation dataset initially consisted of the remaining 137 time periods with convective cells not used in the training dataset. Each of these time periods was analyzed in the same manner as time periods in the training dataset. The heights of the

$-5°$, $-10°$, $-15°$, and $-20°$C levels were recorded, then operationally significant cells with optimal VCPs at the thermal levels of interest were selected for further analysis. The validation cells also required a complete archive of 4DLSS data to determine if and when lightning occurred. After the initial analysis was completed, the validation dataset consisted of 124 cells, with 73 producing lightning and 51 not producing lightning. Each cell in the validation dataset was then analyzed to determine whether or not it achieved one of the 18 thresholds developed from the training dataset. Two thresholds derived from the Pinder Principles were also analyzed to serve as baselines. Based on significance testing using paired t-tests, only the $-5°$C and $-10°$C thermal levels were examined as part of the validation dataset.

If a predictor threshold was exceeded by a particular cell, it was recorded as a hit if the cell produced lightning. If the cell did not produce lightning, it was recorded as a false alarm. For each hit recorded, the time when the entire volume scan completed was recorded as the hit time. These hit times were recorded to the nearest second and then subtracted from the time lightning occurred, providing the lead time of a particular threshold. If a cell did not achieve a threshold set by a predictor, it was considered a miss if the cell produced lightning. If the cell did not produce lightning and did not hit a threshold, it was was recorded as a correct rejection. A summary of the four possible outcomes for any cell within the validation dataset is shown in Table 2.

Table 2. Outcomes of a yes/no forecast based on whether the event is forecasted and whether it is observed. This table was developed from Jolliffe and Stephenson (2003).

Event Forecast	Event Observed	
	Yes	No
Yes	Hit	False Alarm (FA)
No	Miss	Correct Rejection (CR)

3.4 Forecast Metrics

Forecast outcomes and lead times were tallied for each of the 20 predictors tested. These statistics were then compared using a variety of performance measures that evaluated the skill of each lightning prediction method. The hit rate, or POD, was the first measure tested. POD provides the proportion of lightning occurrences that were correctly forecasted (Jolliffe and Stephenson 2003), and is defined as:

$$POD = \frac{Hit}{Hit + Miss} \tag{10}$$

A POD close to 1.0 is desired, since it indicates a forecasting method that is limiting the number of missed forecasts. However, since POD does not take FAs into account, it is limited in measuring the overall skill of a forecast.

Two metrics measure skill based on FAs. The first is FAR, which gives the probability of a FA when an occurrence is forecasted (Jolliffe and Stephenson 2003). FAR is defined as:

$$FAR = \frac{FA}{FA + Hit} \tag{11}$$

An optimal FAR is 0.0, and skill is considered perfect if POD is 1.0 and FAR is 0.0. Like POD, FAR is not a great measure of skill when used alone due to the dependence on the number of hits. Another way to measure FAs is probability of false alarms (PFA), which compares the number of FAs to the number of CRs (Jolliffe and Stephenson 2003) and is defined as:

$$PFA = \frac{FA}{FA + CR} \tag{12}$$

A PFA close to 0.0 is desired, but like FAR, this metric alone is limited in providing a measure of forecast reliability due to the dependence on CR in the denominator.

Three forecast metrics that provide valuable stand-alone information, the CSI, the true skill statistic (TSS), and the operational utility index (OUI) were also calculated. CSI provides the probability of a hit occurring when an event is either forecast, observed, or both (Jolliffe and Stephenson 2003). CSI is defined as:

$$CSI = \frac{Hit}{Hit + FA + Miss} \tag{13}$$

A perfect CSI has a value of 1.0 while values close to 0.0 indicate no skill. The CSI is best used to measure events that occur rarely, but it can still provide value for this study when comparing the overall performance of each lightning forecast method.

The TSS, also known as Peirce's Skill Score, is a metric that takes all the statistics from Table 2 into account. It directly compares the POD with PFA and is defined as:

$$TSS = \frac{(Hit * CR) - (FA * Miss)}{(Hit + Miss)(FA + CR)} \tag{14}$$

TSS can range from -1.0 to 1.0, with values of -1.0 indicating perfect skill but incorrect calibration (Jolliffe and Stephenson 2003). TSS values of 0.0 indicate no skill, while TSS values of 1.0 show perfect skill and proper calibration. TSS can be a reliable metric as long as its dependence on threshold probability is taken into account (Jolliffe and Stephenson 2003). TSS is also used in the calculation of OUI.

OUI was developed at 45 WS, and it is optimized to test the operational utility of lightning prediction algorithms (Roeder 2015). OUI is a non-standard metric that combines POD, PFA, TSS, and average lead time, with a weighting scheme based on 45 WS operational priorities. POD has the largest weight since the ability to detect lightning with a given forecast method is important to personnel safety. TSS has the second highest weight, as it is a good measure of overall skill. PFA has the lowest

weight since the 45 WS accepts some FAs as long as a high POD is maintained. Lead time is also incorporated into the calculation with weighting equal to TSS. In this study, the average lead time of a forecasting algorithm is measured against the 45 WS standard desired lead time of 30 min. OUI is calculated as:

$$OUI = \frac{((3 * POD) + (2 * TSS) + (2 * (LeadTime/30)) + (1 * (1 - PFA)))}{8} \quad (15)$$

An OUI of 1.0 represents perfect performance while a score of 0.0 indicates worthless performance. As the preferred metric of 45 WS, the lightning prediction methods tested in this study with an OUI closest to 1.0 were considered the best for operational forecasting purposes.

IV. Results

This chapter presents the results obtained from the training and validation datasets. The training dataset was analyzed to determine optimal radar-based lightning initiation predictors. Each predictor was then tested on convective cells in the validation dataset. The process of testing each predictor followed similar methods previously used by Woodard (2011) and Thurmond (2014) to determine if a combination of Z and DP parameters could be used as a lightning prediction algorithm that provided increased skill over using Z alone.

The significant difference between this study and the Thurmond (2014) study is that this study examined all types of lightning detected by the 4DLSS system, while the Thurmond study only examined CG lightning. This caused the results and predictors tested as part of this study to differ from those found by Thurmond (2014) since lightning aloft typically occurs before CG lightning. Additionally, some weaker thunderstorms with IC or CC lightning may not even produce CG lightning. In the training dataset, 13 of the 74 lightning-producing storms analyzed did not produce CG lightning. Additionally, lightning aloft occurred well before CG lightning in the training dataset with an median lead time of 4.87 min. Since 45 WS is concerned with the occurrence of all types of lightning, including data from the 4DLSS system brought additional benefit to the predictors examined in this study. The Woodard (2011) study did examine both CG lightning and lightning aloft.

This study analyzed a total of 249 convective cells in the training and validation datasets, compared to sample sizes of 50 examined by Woodard (2011) and 68 examined by Thurmond (2014). The larger sample size likely led to some differences in results. Additionally, this study used a large training dataset to build forecast algorithms, while the other two studies tested multiple predictors across a range of predefined Z and Z_{DR} values. The statistical development of predictors by this study

likely enhanced any dissimilarities encountered between these results and those found by Woodard (2011) and Thurmond (2014).

4.1 Training Dataset Analysis

The initial results from the training dataset were separated by thermal level for analysis. The means of all recorded radar parameters for lightning and non-lightning producing cells were calculated for each time bin and tested for significance against a baseline mean. This baseline was calculated as the overall mean of a parameter for all cells, at all times, for a given thermal level. A paired t-test for dependent variables was used to determine if the means within each time bin had a statistically significant difference from the overall mean. Resulting t-values were tested for significance using a one-tailed test at a 0.05 significance level. Once means for each thermal level, time bin, and parameter were tested for statistical significance, scatter plots comparing Z, Z_{DR}, and K_{DP} were compared to determine which DP parameters to pair with a Z predictor. Results for each thermal level were also normalized so that signal detection charts could be analyzed to estimate the performance of potential predictors to be tested with the validation dataset.

4.1.1 Analysis at −5°C

The lowest height analyzed in the training dataset was −5°C. This was lower than a majority of previous studies examined, including those of Thurmond (2014) and Woodard (2011). The −5°C height typically exists several hundred meters below the main charging region within a cloud, so a majority of lightning formation mechanisms do not occur at this height. However, this level should contain the base of a Z_{DR} column within a developing updraft, and mixed phase hydrometeors. The results at −5°C are displayed in Table 3 and Figure 13.

Table 3. Means and standard deviations (Std Dev) of Z, Z_{DR}, and K_{DP} vs. minutes before lightning initiation for the training dataset analyzed at −5°C. The mean Z t-test results and the significance of the test are shown in the bottom two rows.

Time Bin (Minutes)	45-50	40-45	35-40	30-35	25-30	20-25	15-20	10-15	5-10	0-5
Mean Z	28.89	25.93	26.48	27.84	29.67	30.98	34.06	37.28	42.89	46.40
Std Dev	10.89	9.82	7.65	10.03	10.98	10.18	8.93	7.45	6.88	6.29
Mean Z_{DR}	1.08	1.25	1.33	1.16	1.24	1.27	1.16	1.17	1.32	1.28
Std Dev	1.28	1.41	1.27	1.05	1.25	1.43	1.02	0.88	0.92	1.01
Mean K_{DP}	1.13	-0.29	-0.10	-0.02	0.20	0.36	0.21	0.31	0.35	0.42
Std Dev	0.00	0.57	0.72	0.45	0.76	0.49	0.58	0.67	0.75	0.81
T-Test (Z)	1.54	3.55	5.01	3.65	2.28	1.74	-0.61	-4.46	-11.91	-17.81
Significant	No	No	No	No	No	No	No	Yes	Yes	Yes

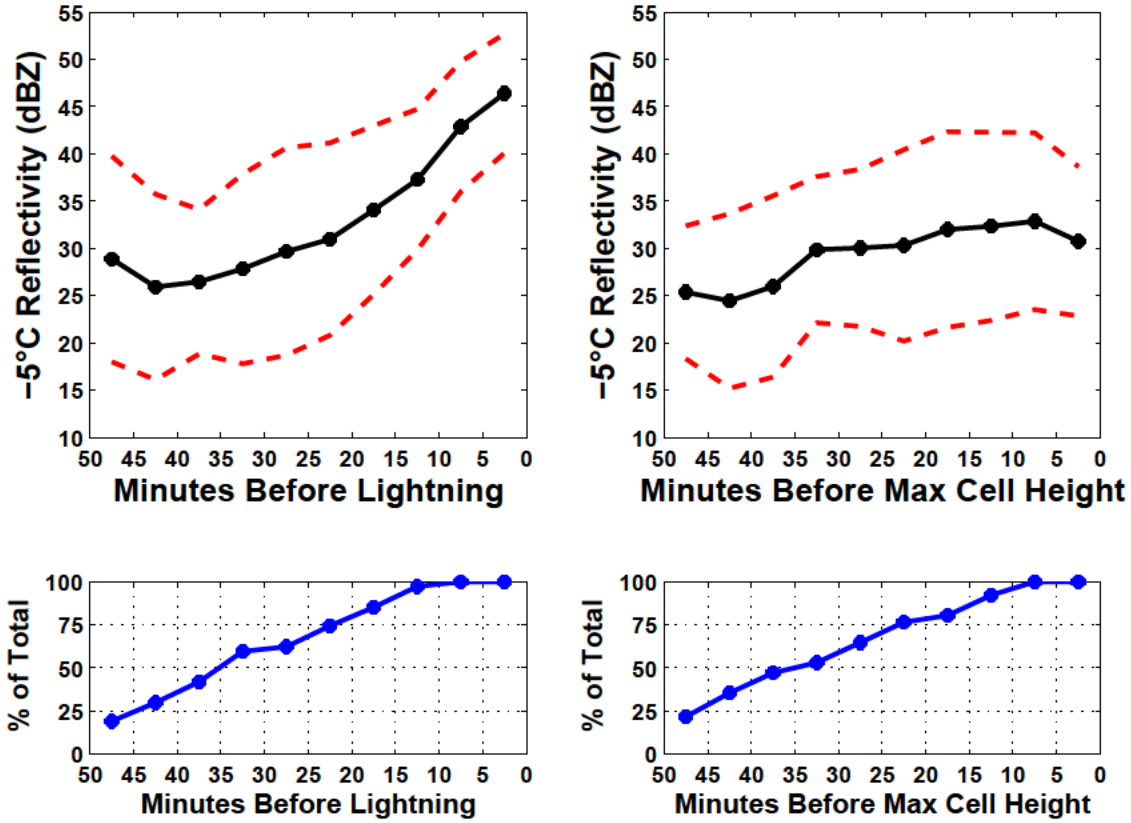

Figure 13. Mean Z at −5°C plotted by time bin for lightning (left) and non-lightning (right) producing cells. The dashed red line is plus or minus one standard deviation. The lower plots depict the fraction of cells with Z above the −5°C level. The chart shows that a noticeable increase in Z occurs 15–20 min before lightning initiation, consistent with the significance test results.

Significance testing revealed that the mean Z in the three time bins before lightning initiation varied significantly above the overall mean of all cells in all time bins. No Z_{DR} or K_{DP} time bins varied significantly from their overall means. Means were also calculated for the first 20 min and first 15 min before lightning initiation, and those combined time bins also had statistical significance. Based on this, predictors at -5°C were targeted for 15–20 min before lightning initiation. The mean Z for all lightning-producing cells in the time bins 0–15 min before lightning initiation was 42.2 dBZ, and the mean Z for all lightning-producing cells in the time bins 0–20 min before lightning initiation was 40.4 dBZ. These two Z values were rounded to the nearest 0.5 dBZ and set as the initial Z predictors to test with the validation dataset.

Scatter plots were created to find ideal combinations of Z and Z_{DR} or K_{DP} to use as DP predictors at -5°C. Linear regression and linear discriminant analyses were performed, but showed limited relationships for developing lightning predictors. This was due to a high concentration of Z_{DR} values of 0.0–1.0 dB for both lightning and non-lightning producing cells. Next, individual time bins were examined to identify any trends before lightning initiation. This technique also proved to be of limited value. Finally, an incremental analysis approach was taken to identify how high to raise a Z_{DR} threshold value to preserve a high lightning POD while limiting FAs.

Since Z had shown significance in the 0–20 min time bins, Z_{DR} was examined incrementally from 0.0–1.0 dB in that time frame to determine a Z_{DR} value that obtained the highest POD with a FAR below 0.20. The target FAR was chosen based on FARs that Thurmond (2014) and Woodard (2011) encountered with their best performing predictors. This approach involved a signal detection model as described by Jolliffe and Stephenson (2003). The detection model used normalized results from the training dataset to predict what a lightning initiation POD and FAR would be for a given Z_{DR} value. This analysis revealed that a Z_{DR} of 0.81 dB was the optimal

threshold to maximize POD while keeping FARs below 0.20. Setting the predictor higher than 0.81 dB would decrease the FAs, but would likely result in decreased lead times and POD. A lower predictor would increase the FAs, but increase lead times and POD. A value of 0.81 dB sought to find a balance between FAR, POD, and lead time. Figure 14 displays a Z_{DR} versus Z scatter plot used as part of this analysis.

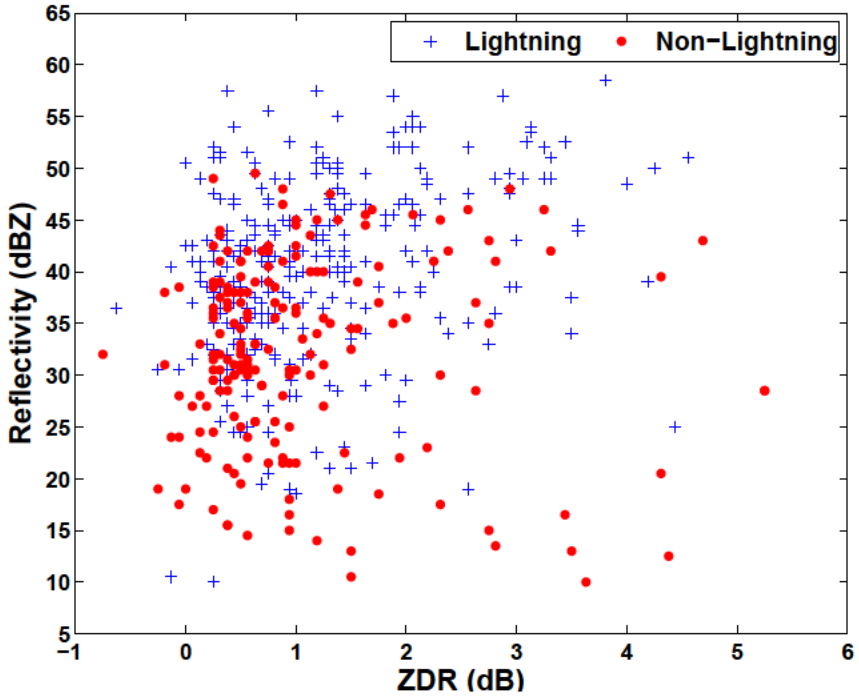

Figure 14. A Z_{DR} versus Z scatter plot at -5°C for all lightning and non-lightning producing cells. A significant amount of plots fall between a Z_{DR} of 0.0 and 1.0 dB for both types of cells. The most usable correlation in this plot is that lightning occurs often with $Z \geq 47.0$ dBZ and Z_{DR} at or above 1.0 dB.

K_{DP} scatter plots also showed little correlation between Z and K_{DP}. There was a concentration of K_{DP} values near $0.0\,^{\circ}\,\mathrm{km}^{-1}$ for lightning and non-lightning producing cells, but it was not possible to set a specific K_{DP} predictor that eliminated non-lightning producing cells while retaining a majority of lightning producers. However, while building the training dataset, analysis revealed that K_{DP} values were typically $0.0\,^{\circ}\,\mathrm{km}^{-1}$ or unreported by the WSR-88D until Z reached 35.0 dBZ due to the measured phase shift being minimal unless a significant amount of hydrometeors

were present within a volume. Based on this and the scatter plot data, validation predictors were set to use any cells registering non-zero K_{DP} values above a certain Z value. Additionally, though it would not work as an unique predictor due to low POD expectations, analysis indicated lightning almost always occurred with $K_{DP} \geq 1.0\,^{\circ}\,\mathrm{km}^{-1}$. A K_{DP} versus Z scatter plot used for this analysis is shown in Figure 15.

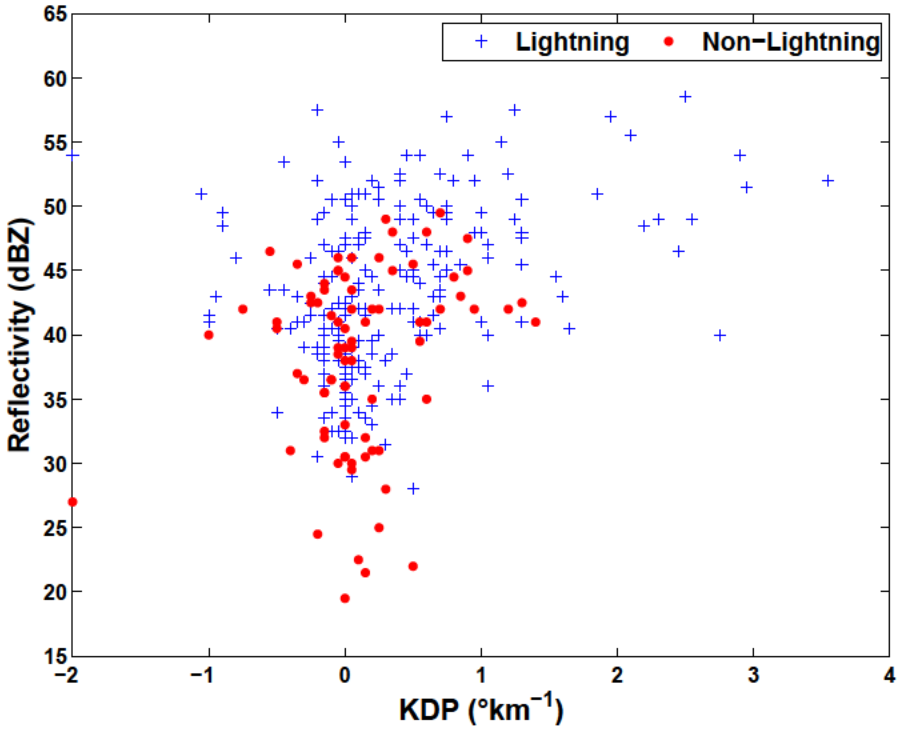

Figure 15. A K_{DP} versus Z scatter plot at -5°C for lightning and non-lightning producing cells 0–20 min before lightning initiation or maximum cell intensity. Plots were not created for time bins when K_{DP} data was not available. There are limited correlations in this plot as both types of cells have K_{DP} values near 0.0 °km^{-1} for all Z values. This plot does show that lightning is likely when Z is above 45.0 dBZ and K_{DP} is above 0.0 °km^{-1}.

Scatter plots were also created to analyze relationships between K_{DP} and Z_{DR}, but showed no usable correlations. However, combining K_{DP} and Z_{DR} would add an extra requirement that could lower the number of FAs. It was also observed that lightning was likely to occur when Z exceeded 46.0 dBZ, regardless of K_{DP} or Z_{DR}. When all potential predictors were identified, signal detection models based on Jolliffe and Stephenson (2003) were once again examined to predict FARs for a given

predictor. The signal detection curves revealed that the initial predictors established using significance testing and scatter plot analysis would result in FARs at or below 0.20. This was deemed acceptable as it was consistent with results found by the Thurmond (2014) and Woodard (2011) studies. The complete Z, K_{DP}, and Z_{DR} analysis was then used to establish nine lightning initiation predictors at the $-5°C$ height to test against the baseline established by the Pinder Principles. Figure 16 depicts a basic signal detection model plot used for this analysis.

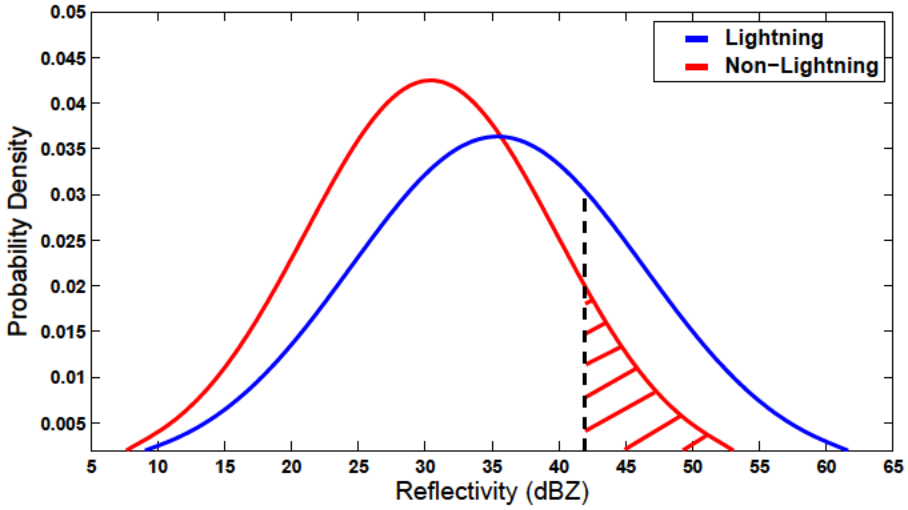

Figure 16. Several signal detection plots were created to predict FARs based on proposed Z and DP predictors. This plot contains normalized Z curves for lightning and non-lightning cells at $-5°C$. The dashed black line is a proposed Z predictor of 42.0 dBZ. This results in an FAR of 0.11, which is represented by the hatched red area.

4.1.2 Analysis at $-10°C$

Previous research, including the Thurmond (2014) and Woodard (2011) studies, showed promising results using the $-10°C$ height. Thurmond (2014) showed that $Z \geq 30.0$ dBZ combined with $Z_{DR} \geq 0.5$ dB at $-10°C$ produced the most desirable results for an operational user due to a high skill score and lead time in excess of 15 min. This height lies at the lower edge of the charging region within the cloud. This is also the level of interest in the Pinder Principles. The results at $-10°C$ are displayed in Table 4 and Figure 17.

Table 4. Means and standard deviations (Std Dev) of Z, Z_{DR}, and K_{DP} vs. minutes before lightning initiation for the training dataset analyzed at −10°C. The mean Z t-test results and the significance of the test are shown in the bottom two rows.

Time Bin (Minutes)	45-50	40-45	35-40	30-35	25-30	20-25	15-20	10-15	5-10	0-5
Mean Z	24.72	24.00	23.50	22.98	23.42	25.55	27.69	31.32	37.18	41.04
Std Dev	7.75	8.59	7.15	9.16	9.27	7.09	8.98	7.15	6.86	6.19
Mean Z_{DR}	1.37	1.06	0.95	0.70	1.14	0.97	0.92	0.89	0.96	0.86
Std Dev	1.87	0.83	1.06	0.87	1.62	1.42	0.94	0.75	0.89	0.83
Mean K_{DP}	–	-0.40	-0.05	-0.07	0.03	0.03	0.33	0.11	0.13	0.15
Std Dev	–	–	–	0.12	0.19	0.31	0.67	0.53	0.60	0.51
T-Test (Z)	0.25	2.15	3.51	3.25	3.27	3.10	1.15	-2.55	-9.98	-16.59
Significant	No	No	No	No	No	No	No	Yes	Yes	Yes

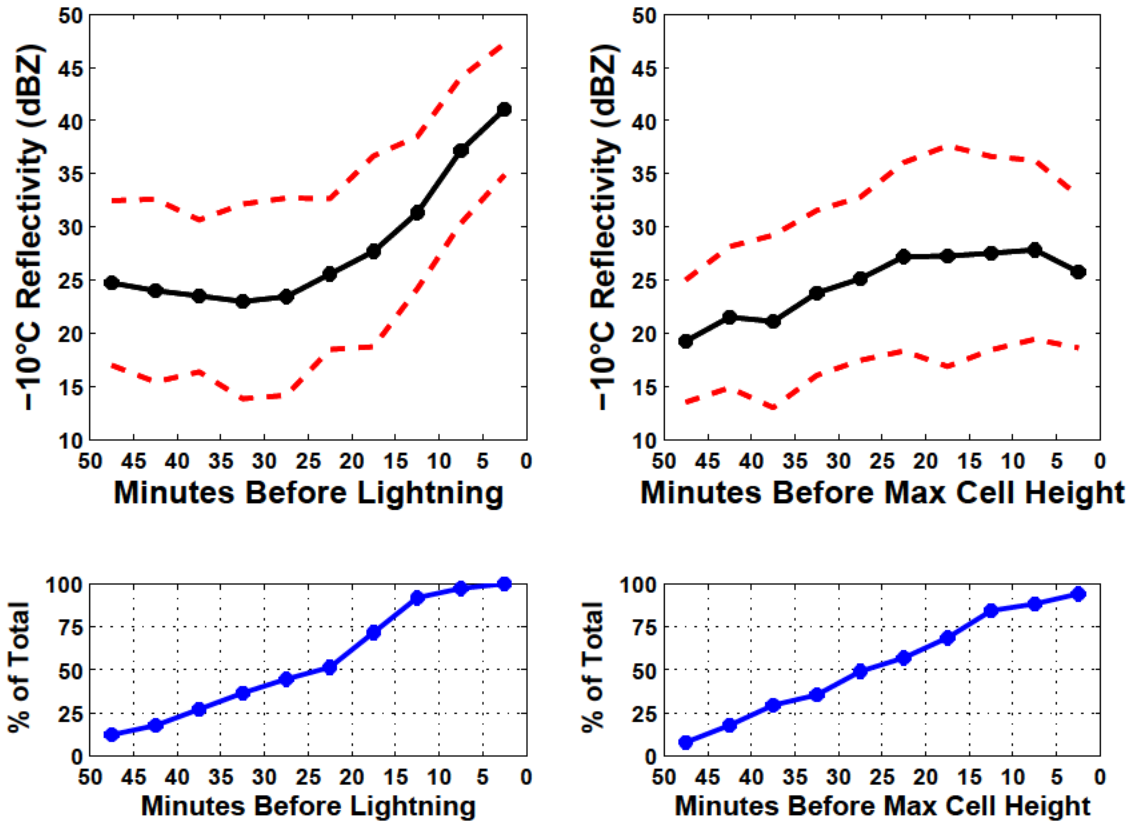

Figure 17. Mean Z at −10°C plotted by time bin for lightning (left) and non-lightning (right) producing cells. The dashed red line is plus or minus one standard deviation. The lower plots depict the fraction of cells with Z above the −10°C level. The chart shows that a noticeable increase in Z occurs 10–15 min before lightning initiation, consistent with the significance test results.

The $-10°$C results were very similar to those at $-5°$C. Significance testing showed that the mean Z values in the three time bins before lightning initiation varied significantly above the overall mean for all cells in all time bins. Mean values of Z_{DR} or K_{DP} did not show any statistical significance. Mean Z values were also calculated for both time bins 15 and 20 min before lightning initiation. These two means also showed significance above the overall mean. The two means were chosen as Z predictors to be used for validation based on their significance and potential lead times. The mean, rounded to the nearest half, was 36.5 dBZ for all lightning-producing time bins 0–15 min before lightning initiation, and the mean was 35.0 dBZ for the 0–20 min time bins.

Scatter plots were created at the $-10°$C height to identify any correlations between Z, K_{DP}, and Z_{DR}. The Z_{DR} scatter plots showed no significant correlations, as a majority of Z_{DR} values for both lightning and non-lightning producing cells fell between 0.0 and 1.0 dB for all time bins. Thurmond (2014) found success setting a Z_{DR} predictor at 1.0 dB, but based on the training dataset, such a high predictor would severely reduce POD due to mean Z_{DR} values being below 1.0 dB less than 25 min before lightning initiation. Thurmond (2014) and Woodard (2011) also saw improved skill scores when setting a Z_{DR} predictor at 0.5 dB. This value was considered, but with a mean Z_{DR} of 0.91 dB and standard deviation of 0.84 dB for the four time bins before lightning initiation, the resulting z-score of -0.47 would only result in a POD of 0.68. This would lower the FAR, but the POD would likely be unacceptable to operational users. A lower of 0.31 dB was chosen as a predictor after completing the same analysis processes used for $-5°$C. Linear regression and linear discriminant analyses showed no usable correlations, but signal detection models showed that a Z_{DR} of 0.31 dB provided a predicted POD of 0.77, while maintaining a FAR below 0.20. Figure 18 displays a Z_{DR} versus Z scatter plot used as part of this analysis.

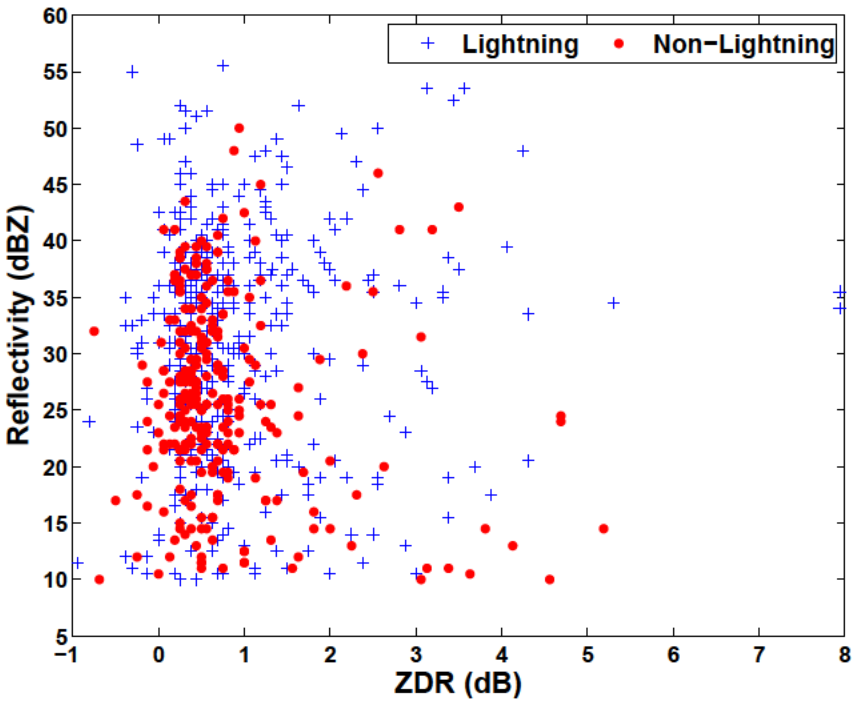

Figure 18. A Z_{DR} versus Z scatter plot at −10°C for all lightning and non-lightning producing cells. A significant amount of plots fall between a Z_{DR} of 0.0 and 1.0 dB for both types of cells. The most usable correlation in this plot is that lightning occurs much more often with $Z \geq 37.0$ dBZ and Z_{DR} at or above 0.75 dB.

The K_{DP} scatter plots also showed no discernible correlation between Z and K_{DP}. Much like at −5°C, K_{DP} values were typically not available until Z exceeded 35.0–40.0 dBZ. Also, only 25 of 74 lightning-producing cells even had non-zero K_{DP} values 10 min before lightning initiation. This made it unlikely that a specific K_{DP} value could be useful at −10°C. However, only 10 out of the 74 lightning-producing cells never produced non-zero K_{DP} values, so a predictor was set to use any value of K_{DP}. Additionally, though it would not work as an individual predictor, lightning almost always occurred when K_{DP} was greater than $0.1\,^{\circ}\,\mathrm{km}^{-1}$. Scatter plots were also created to analyze relationships between K_{DP} and Z_{DR} at −10°C, but showed no correlations. However, when Z exceeded 40.5 dBZ, lightning was likely to occur, independent of K_{DP} or Z_{DR}. A K_{DP} versus Z scatter plot used as part of this analysis is displayed in Figure 19.

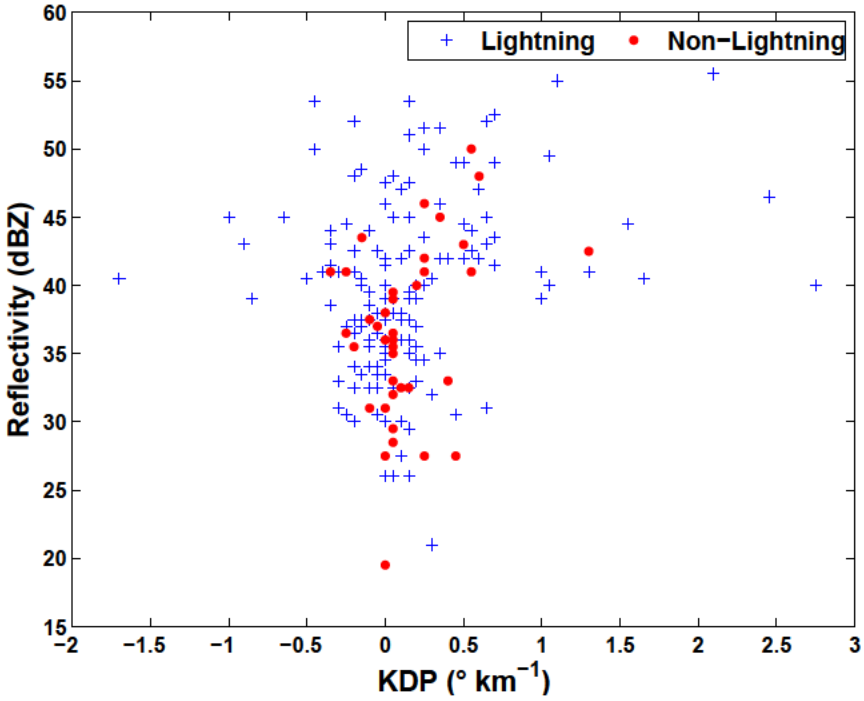

Figure 19. A K_{DP} versus Z scatter plot at $-10°$C for all lightning and non-lightning producing cells. There are limited correlations in this plot as both types of cells have K_{DP} values near 0.0 °km^{-1} for all Z values.

Additional signal detection model plots were also created at $-10°$C to predict FARs of individual and combined Z and DP predictors developed using significance testing and scatter plot analysis. The predicted FARs for all the potential predictors fell below 0.20, which was considered acceptable based on previous studies. A total of nine different predictors at $-10°$C were established to test against the baseline.

4.1.3 Analysis at $-15°$C

The $-15°$C level lies at the mean height of the main charging region. Developing convective cells typically have a large concentration of mixed hydrometeros and a net negative charge at this height. Thurmond (2014) discovered the highest skill score at the $-15°$C level by setting a predictor of $Z \geq 35.0$ dBZ combined with $Z_{DR} \geq 0.5$ dB. Woodard (2011) also found the best predictor based on skill score to be $Z \geq 40.0$ dBZ at $-15°$C. The results at $-15°$C are displayed in Table 5 and Figure 20.

Table 5. Means and standard deviations (Std Dev) of Z, Z_{DR}, and K_{DP} vs. minutes before lightning initiation for the training dataset analyzed at −15°C. The mean Z t-test results and the significance of the test are shown in the bottom two rows.

Time Bin (Minutes)	45-50	40-45	35-40	30-35	25-30	20-25	15-20	10-15	5-10	0-5
Mean Z	18.08	23.64	20.71	21.94	22.59	21.12	23.56	26.04	31.13	35.74
Std Dev	8.63	9.78	5.75	8.01	7.93	8.21	7.98	7.24	6.16	6.58
Mean Z_{DR}	0.96	0.80	0.81	0.66	1.04	1.20	0.96	0.82	0.79	0.64
Std Dev	1.55	0.39	0.87	0.85	1.75	1.51	1.07	0.77	0.68	0.63
Mean K_{DP}	–	-0.40	–	0.05	-0.15	-0.15	0.10	-0.03	0.04	0.06
Std Dev	–	–	–	–	0.21	0.15	0.15	0.11	0.20	0.35
T-Test (Z)	3.78	-0.25	3.14	2.65	1.64	2.40	0.89	-0.20	-4.93	-8.84
Significant	No	No	No	No	No	No	No	No	Yes	Yes

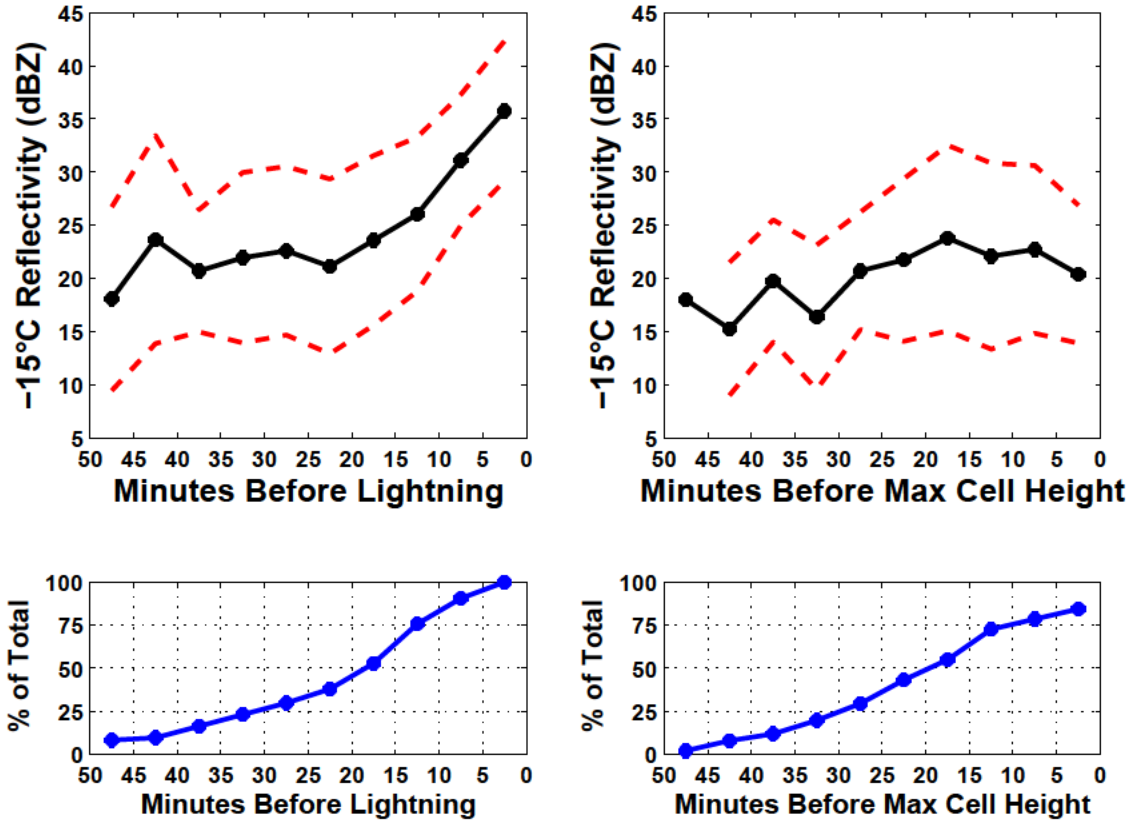

Figure 20. Mean Z at −15°C plotted by time bin for lightning (left) and non-lightning (right) producing cells. The dashed red line is plus or minus one standard deviation. The lower plots depict the fraction of cells with Z above the −15°C level. The chart shows that a noticeable increase in Z occurs just 5–10 min before lightning initiation, consistent with the significance test results. Also, only about 50% of lightning-producing cells even extended to the −15°C height 15–20 min before lightning occurred.

Significance testing at −15°C showed that the mean Z values in just the first two time bins before lightning initiation varied significantly above the overall mean of every cell in all time bins at this level. As a result, any predictors created using the −15°C height could not be expected to exceed an average lead time of 10 min. Using a predictor for lightning aloft of 40.0 dBZ at −15°C, Woodard (2011) was able to achieve perfect POD, CSI, and FAR of 0.0. However, the average lead time was only 8 min. That lead time corresponds with significance testing results at this height, and suggests that any predictors set using this thermal level would have a high POD, but average lead times of only 5–10 min.

Since operators at KSC/CCAFS/PAFB desire 30 min of lead time before lightning occurs, any predictors derived from these results would fall well short of operational requirements. Additionally, only 75.7% of lightning-producing cells even reached the −15°C height 10–15 min before lightning initiation, which would likely cause lead times at this level to be shorter than those provided by the Pinder Principles. Finally, analysis combining Z with Z_{DR} or K_{DP} data at this level showed limited correlations or trends that could be used as lightning predictors. As a result, no predictors were created for validation at −15°C.

4.1.4 Analysis at −20°C

The highest height analyzed as part of the training dataset was −20°C. This height is the top of the cloud charging region and ice crystals become dominant hydrometeors at this level. Woodard (2011) examined predictors using the −20°C height, but found that lead times were greatly diminished due to lightning typically occurring shortly after a convective cells extends above −20°C. The results at −20°C are displayed in Table 6 and Figure 21.

Table 6. Means and standard deviations (Std Dev) of Z, Z_{DR}, and K_{DP} vs. minutes before lightning initiation for the training dataset analyzed at −20°C. The mean Z t-test results and the significance of the test are shown in the bottom two rows.

Time Bin (Minutes)	45-50	40-45	35-40	30-35	25-30	20-25	15-20	10-15	5-10	0-5
Mean Z	14.00	19.25	20.50	18.05	18.14	18.82	20.54	21.83	25.25	31.15
Std Dev	4.95	3.77	4.61	6.39	6.41	7.36	8.43	7.02	7.96	7.64
Mean Z_{DR}	0.82	0.25	0.34	0.38	0.79	0.77	0.69	0.64	0.76	0.68
Std Dev	0.88	0.06	0.33	0.35	0.56	1.35	0.78	0.74	0.72	0.60
Mean K_{DP}	–	–	–	0.20	0.10	0.10	0.00	0.02	0.06	0.11
Std Dev	–	–	–	–	–	–	0.13	0.08	0.10	0.30
T-Test (Z)	9.13	4.72	2.53	3.27	2.84	3.05	1.47	0.40	-1.53	-5.81
Significant	No	No	No	No	No	No	No	No	No	Yes

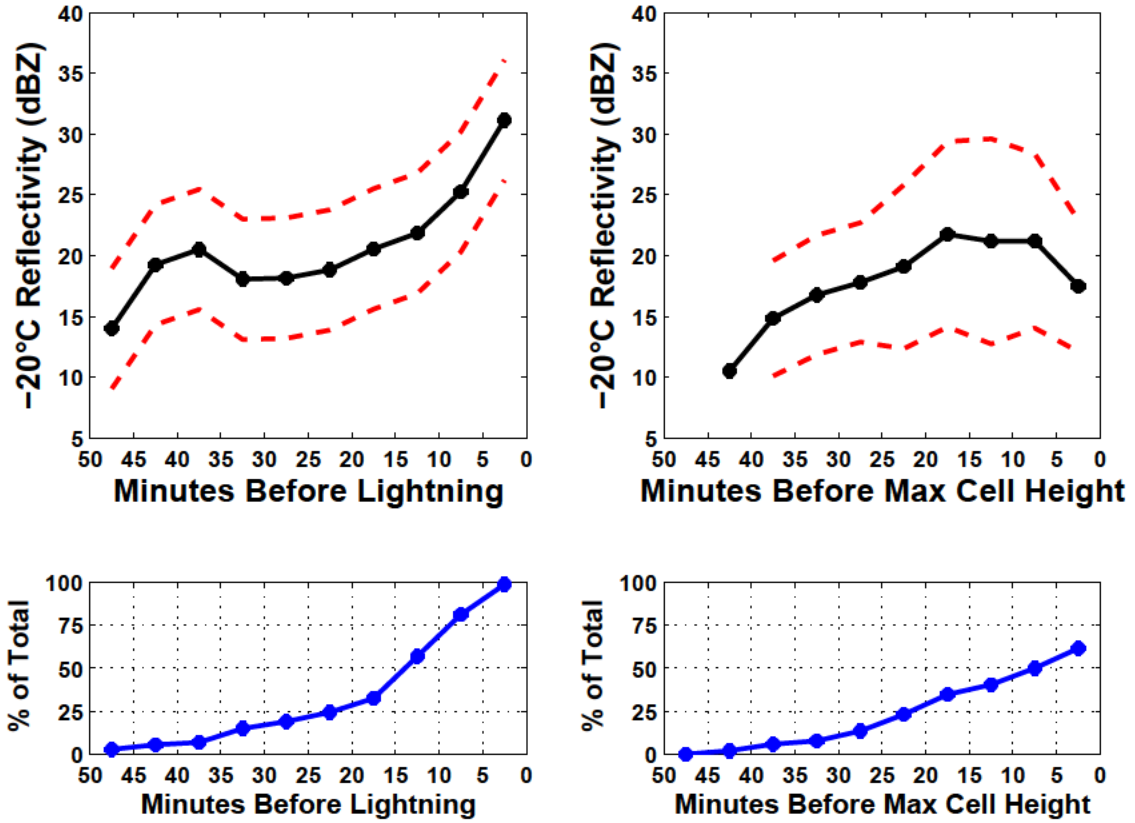

Figure 21. Mean Z at −20°C plotted by time bin for lightning (right) and non-lightning (left) producing cells. The dashed red line is plus or minus one standard deviation. The lower plots depict the fraction of cells with Z above the −20°C level. The chart shows that a noticeable increase in Z occurs just 5–10 min before lightning initiation, consistent with the significance test results. Also, only about 30% of lightning-producing cells even extended to the −20°C height 15–20 min before lightning occurred.

Significance testing showed that the mean Z for lightning-producing cells at −20°C only varied significantly from the overall mean during the 0–5 min time bin. Additionally, only 81.1% of lightning-producing cells reached the −20°C height 5–10 min before lightning initiation. One cell even produced lightning before it reached −20°C. Based on this, and a lack of any DP correlations at this level, −20°C was not used to create any predictors. The results did show that when the −20°C height contains a $Z \geq 29.0$ dBZ, lightning always occurs. However, this predictor would indicate lightning is imminent and the expected lead time would be less than 5 min.

4.2 Validation Dataset Results

The validation dataset was used to test a total of 18 lightning prediction algorithms against two baselines. The Pinder Principles for lightning aloft require a cell to have $Z \geq 37.0$ dBZ above the −10°C height with that Z value having a vertical extent of 3000 ft and width of 1.0 nm within a cell. This predictor served as one baseline, while a second baseline was created by removing the 1.0 nm requirement. The two baselines were initially tested to determine the utility of the 1.0 nm width requirement. These baseline results are shown in Table 7.

Table 7. The results of the baseline predictors derived from the Pinder Principles tested at −10°C. The predictor without a width requirement performed the best based on OUI.

−10°C Height Baselines	POD	FAR	CSI	Average Lead Time	Median Lead Time	OUI
37.0dBZ/1nm Width	0.740	0.053	0.711	07:53	05:18	0.631
37.0dBZ	0.849	0.101	0.775	11:42	06:28	0.702

The baseline skill scores were calculated using the 73 lightning and 51 non-lightning producing cells from the validation dataset. The baseline of $Z \geq 37.0$ dBZ at −10°C had increased skill scores and lead times when the 1.0 nm width requirement was removed. The 1.0 nm width lowered the FAR, as it required a cell to have

a large area of elevated Z, but that stringent width requirement would be limited for operational usage due to decreased POD, lead time, and OUI. As the best performing baseline, $Z \geq 37.0\,\text{dBZ}$ at $-10°\text{C}$ was used as the standard to compare against the 18 predictors derived from the training dataset. The results of eight predictors tested at $-5°\text{C}$ are displayed in Table 8. The ninth predictor, which required $Z \geq 40.0\,\text{dBZ}$, $Z_{DR} \geq 0.81\,\text{dB}$ and any K_{DP} value or $Z \geq 40.5\,\text{dBZ}$ with $K_{DP} \geq 1.0\,^{\circ}\,\text{km}^{-1}$ was omitted from Table 8 due to the $K_{DP} \geq 1.0\,^{\circ}\,\text{km}^{-1}$ predictor having no effect on the results.

Table 8. The results of the predictors tested at −5°C. The best performing predictor, based in OUI, is in bold.

−5°C Height Predictors	POD	FAR	CSI	Average Lead Time	Median Lead Time	OUI
40.5dBZ/1nm Width	0.822	0.143	0.723	10:49	07:23	0.655
40.5dBZ	0.918	0.212	0.736	13:27	10:38	0.678
40.5dBZ/.81Z_{DR}	0.890	0.177	0.747	12:43	10:27	0.685
40.5dBZ/.81Z_{DR} or 46.5dBZ	0.890	0.177	0.747	12:46	10:27	0.685
42.0dBZ/.81Z_{DR}	0.849	0.151	0.738	12:30	09:59	0.679
40.5dBZ/AnyK_{DP}	0.918	0.202	0.744	13:11	10:28	0.683
42.0dBZ/AnyK_{DP}	0.890	0.188	0.739	12:28	08:41	0.675
40.5dBZ/.81Z_{DR}/AnyK_{DP}	**0.890**	**0.167**	**0.756**	**12:29**	**09:31**	**0.690**

Predictors tested at the $-5°\text{C}$ height all had lower skill than the standard, as measure by CSI and OUI. All but one predictor had a POD higher than the standard, but this came at a cost of higher FARs. Average lead times were also higher for most of the predictors, while several median lead times bested the standard by over 4 min. Based on these results, predictors at $-5°\text{C}$ are potentially useful if maximum lead time and a high POD is desired at the cost of an increased FAR. By providing over 13 min of average lead time, two of the predictors nearly meet 50% of the lead time desired by operators at KSC/CCAFS/PAFB.

Overall, these results were expected by analysis performed using the training dataset. In most cases, a cell will exhibit increasing Z values at $-5°\text{C}$ as it develops

and expands to greater heights, which can allow for lightning to be predicted with substantial lead time before the storm develops vertically into the main charging zone around the −15°C height. However, some non-lightning producing cells can develop enhanced Z, Z_{DR}, and K_{DP} values at −5°C without the cell expanding upward into the main charging region, leading to increased FARs. To lower the FAR, the Z and/or Z_{DR} of the predictors would have to be raised at a cost of lower POD and lead times, or in this case, a higher height in the atmosphere would have to be examined. The results of eight predictors tested at the −10°C height are shown in Table 9. As with the −5°C level, the $Z \geq 35.0$ dBZ, $Z_{DR} \geq 0.31$ dB and any K_{DP} or $Z \geq 35.0$ dBZ with $K_{DP} \geq 0.1\,^{\circ}\,\mathrm{km}^{-1}$ predictor was omitted from Table 9 due to the $K_{DP} \geq 0.1\,^{\circ}\,\mathrm{km}^{-1}$ predictor causing no change to the results.

Table 9. The results of the predictors tested at −10°C. The best performing predictor, based in OUI, is in bold.

−10°C Height Predictors	POD	FAR	CSI	Average Lead Time	Median Lead Time	OUI
35.0dBZ	0.918	0.163	0.779	12:09	07:29	0.704
36.5dBZ	0.918	0.118	0.817	11:39	06:19	0.730
35.0dBZ/.31Z_{DR}	0.904	0.143	0.786	12:09	07:34	0.710
36.5dBZ/.31Z_{DR}	**0.890**	**0.058**	**0.844**	**11:45**	**06:36**	**0.750**
35.0dBZ/.31Z_{DR} or 41.0dBZ	0.890	0.122	0.793	12:16	07:38	0.718
35.0dBZ/AnyK_{DP}	0.795	0.065	0.753	09:53	05:28	0.675
36.5dBZ/AnyK_{DP}	0.775	0.083	0.724	09:56	05:18	0.657
35.0dBZ/.31Z_{DR}/AnyK_{DP}	0.795	0.049	0.763	09:53	05:28	0.682

Several predictors tested at the −10°C height outperformed the standard, as measured by CSI and OUI skill scores. Predictors that used Z alone or a combination of Z and Z_{DR} outperformed the standard, while predictors using K_{DP} did not. This confirmed the results of Thurmond (2014) who determined that K_{DP} had little utility in predicting lightning initiation. The best performing predictor of all 18 tested, $Z \geq 36.5$ dBZ with $Z_{DR} \geq 0.31$ dB, was at this level. This predictor exceeded the standard based on all performance metrics and skill scores calculated, but only improved the

average lead time by 3 s above the standard. The results at this level and at −5°C both showed a strong relationship between FAR and lead time, which is shown in Figure 22.

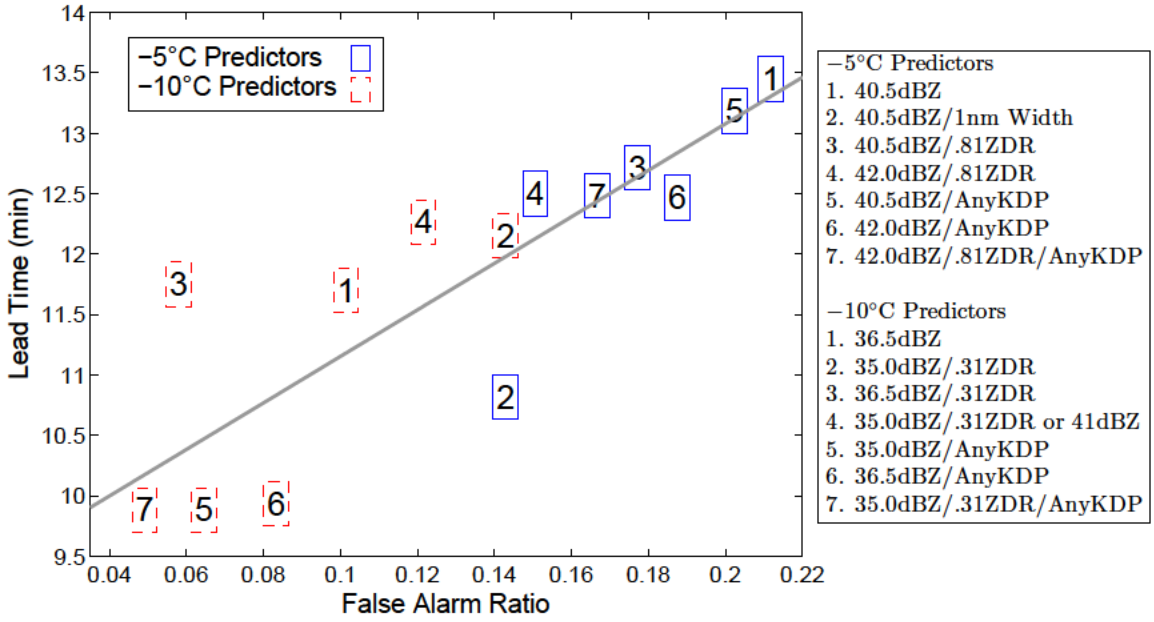

Figure 22. A comparison between FAR and lead time for 14 select predictors at −5°C and −10°C. The gray line is a linear best fit of the plots.

Figure 22 illustrates that predictors must sacrifice an increase in FAR in order to improve lead time. This plot also clearly shows that the $Z \geq 36.5$ dBZ and $Z_{DR} \geq 0.31$ dB at −10°C is the best performing predictor, as it is an outlier above the best fit line (meaning it has a low FAR and high lead time). This same trend also occurs with POD since predictors with the highest PODs also have decreased lead times. Overall, these relationships show that performance offsets between skill and lead time occur when using DP radar to predict lightning initiation. It also illustrates the limits of forecast lead times that DP radar can provide. A closer examination of this is shown in Figure 23. This plot shows how long a lightning-producing cell from the training dataset was continuously visible on radar at the −5°C height before

lightning occurred. The average storm did not even penetrate the −5°C level until 30.2 min before lightning initiation. Based on this information and the significance testing performed in this study, lead times using radar based predictors will likely never exceed 20 min while still maintaining FARs below 0.4.

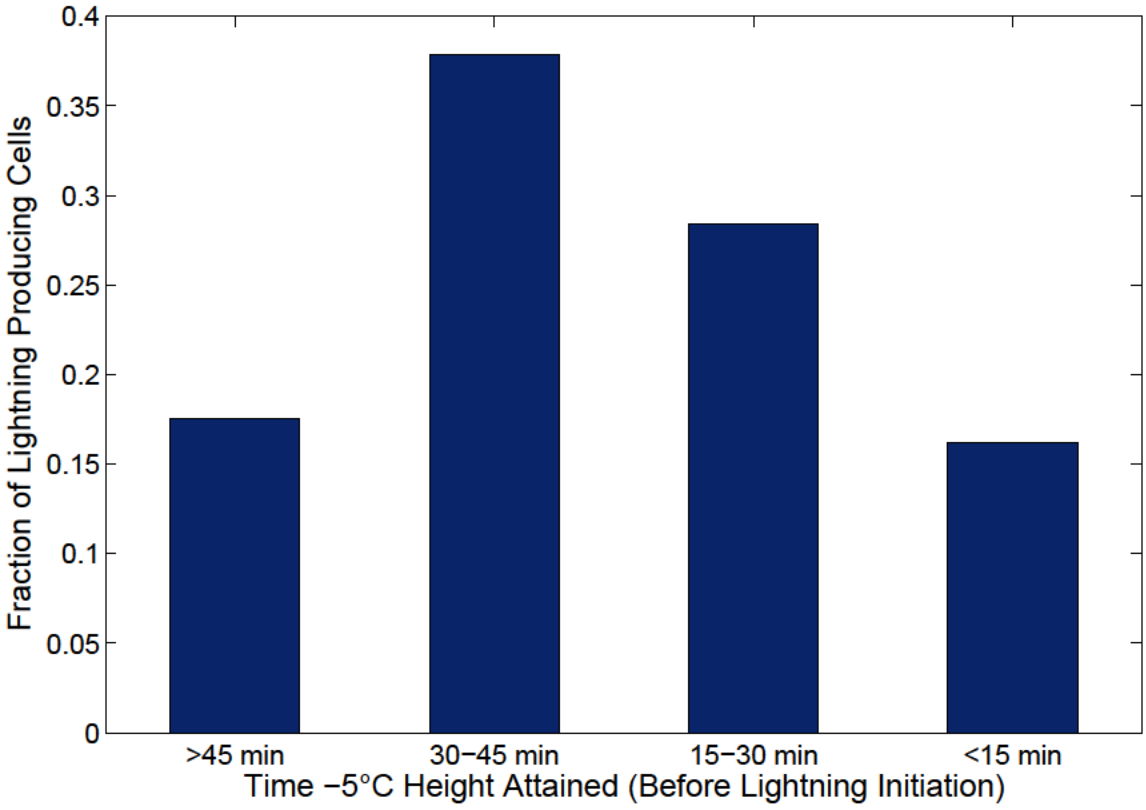

Figure 23. Amount of time before lightning initiation a cell from the training dataset was continuously above the −5°C height.

Finally, the results of this study were similar to those found by Thurmond (2014) and Woodard (2011). Based on their results, a combination of Z and Z_{DR} at −10°C was expected to be the best overall predictor and K_{DP} was expected to be of little value. Both these expectations turned out to be the case, and for comparison, results of similar predictors used by Thurmond (2014) and Woodard (2011) are displayed in Table 10.

Table 10. Select results from the Woodard (2011) and Thurmond (2014) studies. The OUI values in this table were recalculated to match the OUI formula used in this study. Due to recent changes to the OUI formula made by 45 WS, the OUI values in this table do not match the results found in Woodard (2011) or Thurmond (2014).

Reference	-10°C Height Predictors	POD	FAR	CSI	Average Lead Time	OUI
Woodard (2011)	35.0dBZ	1.000	0.244	0.756	12:30	0.657
	40.0dBZ	1.000	0.205	0.795	10:30	0.680
	40.0dBZ/.50Z_{DR}	0.968	0.167	0.811	11:00	0.703
Thurmond (2014)	40.0dBZ	0.957	0.241	0.733	14:33	0.606
	35.0dBZ/.50Z_{DR}	1.000	0.233	0.767	16:47	0.651

The results from Woodard (2011) serve as a better comparison to the results found in this study since lightning aloft data was utilized. The only common predictor used by this study and Woodard (2011) was $Z \geq 35.0\,\text{dBZ}$ at -10°C. This study found similar results, with all forecast metrics and skill scores differing by less than 10%. Woodard (2011) also found increased success by combining Z and Z_{DR} predictors, though the analysis and results of this study show that a Z of 40.0 dBZ is too high of a threshold to use for lightning aloft in Florida. The Thurmond (2014) predictor in Table 10 that utilized Z_{DR} appears to bring a substantial increase in average lead time. However, since that result was obtained using CG lightning, approximately 5.0 min should be subtracted from the average lead time to account for the average time lightning aloft typically occurs before CG lightning. Although changing the lead time alone does not accurately reflect the overall effect lightning aloft would have on the Thurmond (2014) predictors, the results are still comparable to those found by Woodard (2011) and this study.

V. Conclusions

5.1 Summary

The high frequency of thunderstorms along Florida's Space Coast is a significant hindrance to daily operations at KSC, CCAFS, and PAFB. Lightning is a leading cause of launch delays, can bring ground-operations to a standstill, and is a safety hazard for over 25 000 personnel. 45 WS has the challenging responsibility of mitigating the impacts of lightning by accurately forecasting the timing and location of thunderstorms up to 30 min before they occur.

Weather radar is the primary tool used by 45 WS forecasters for short-term lightning prediction. The Pinder Principles, developed at 45 WS, provide empirical guidelines for lightning initiation forecasting using weather radar, but they were developed prior to the advent of DP radar, which was implemented on the KMLB WSR-88D in 2012. DP provides a new tool to examine the size and shape of hydrometeors within a developing thunderstorm. That information can then be utilized to develop new lightning prediction techniques. Studies by Woodard (2011) and Thurmond (2014) both showed that a combination of Z and Z_{DR} predictors can improve forecast skill over methods that utilized Z alone.

This study also confirmed that DP added skill to lightning initiation forecasts. The best performing predictor in this study, $Z \geq 36.5$ dBZ with $Z_{DR} \geq 0.31$ dB at -10°C, improved upon the standard method using $Z \geq 37.0$ dBZ at -10°C by 6.8% as measured by OUI. While this increase in OUI is somewhat limited, even small improvements do have a positive impact on overall facility and personnel safety. By including a Z_{DR} predictor with Z, it led to increased POD and lead time while decreasing the FAR. The analysis also showed that a Z_{DR} predictor allowed a lower Z threshold to be set, improving the overall POD and lead time without the cost of

higher FARs. These thresholds can also can be altered depending on user requirements with the understanding that attempts to increase POD or lead time will also increase the FAR.

The best results in terms of average and median lead times were found using predictors at −5°C. These predictors did not improve OUI over the standard due to increased FAs, but median lead times bested the standard and the top performing predictor of this study by over 4 min. Combining a $Z \geq 40.5$ dBZ with a Z_{DR} and/or K_{DP} threshold led to these increased lead times while maintaining an OUI within 2% of the standard. Depending on operator requirements, that extra 4 min of lead time may be worth the 7% increase in FAR. Additionally, further adjustment of the predictors could bring additional increases in lead time depending on what FAR is deemed acceptable. However, targeting lead times in excess of 20 min for all types of lightning would likely not be feasible as 26% of lightning-producing cells analyzed as part of the training dataset formed and generated lightning in 30 min or less.

The results showed that Z_{DR} is the preferred DP parameter to use in combination with Z to improve lightning prediction. This is due to elevated Z_{DR} values being indicative of supercooled water droplets and wet ice particles. Within a developing convective updraft, those mixed phase hydrometeors contribute to cloud charging and create a Z_{DR} column as discussed by Kumjian (2013b). However, the presence of the Z_{DR} column alone does not indicate imminent lightning, as nearly all the non-lightning producing cells that exceeded the −15°C height also contained updrafts with a column of elevated Z_{DR}. K_{DP} achieved some success as a predictor at −5°C, but the training set data showed that it would be very difficult to set a specific K_{DP} threshold without significantly lowering POD. Additionally, using K_{DP} as a predictor at −5°C in combination with $Z \geq 40.5$ dBZ only achieved marginal improvement over employing $Z \geq 40.5$ dBZ alone.

5.2 Recommendations for Future Work

To increase the overall confidence level of this study, additional convective cells need to be included in the training dataset. If a 95% confidence level is desired, the means calculated at −5°C using the existing training dataset have a confidence interval of ±1.8 dBZ. To bring the confidence interval under 1.0 dBZ, it would require a sample size of 420 convective cells. If a confidence interval below 0.5 dBZ was desired, it would require over 1700 convective cells to be analyzed.

Analyzing that many convective cells would likely not only require a longer archive of DP data, but would also require an improved automation process. To automate the analysis performed on the training dataset, a Storm Cell Identification and Tracking (SCIT) algorithm could be developed. This technique was used by the Mosier et al. (2011) lightning initiation study that analyzed 67 384 unique convective cells. Further details on developing a SCIT algorithm are discussed by Johnson et al. (1998), but the time and coding required to incorporate LDAR and DP radar data into a SCIT algorithm goes well beyond the scope of this study.

This study could also be expanded by including DP data from the TDR 43-250 used by 45 WS. Over the next year or two, enough archived TDR 43-250 data should be available to build a database that could expand this study. The advantage of using this radar over the KMLB WSR-88D is that its scan elevation angles are optimized for coverage over KSC/CCAFS. The scan elevation angles can also be modified locally by 45 WS so that specific thermal levels could be targeted to verify or improve the results of this study. The TDR 43-250 also operates using the C-Band (5.33 cm), which would provide higher resolution data for future studies. The TDR 43-250 could also test other levels, such as −7.5°C, to determine if it might balance the improved lead times at −5°C with the best performing OUI results at −10°C. More consideration to specific thermal levels could also be explored to take into account

how the temperature levels within a convective cell lower during the developing stage due to evaporational cooling.

Future studies could also focus on creating additional predictors or expanding the study to other geographical regions. New predictors that include PID algorithms could be considered, especially since these algorithms continue to improve as a result of new research and in situ verification projects. Additional predictors that require thresholds to be met for consecutive volume scans or at multiple thermal levels may also improve results. Expanding the study to new geographical areas would increase the number of cells available for testing and determine if the predictors from this study would perform as well in mountainous or inland plains regions. To perform this research, lightning mapping arrays (LMAs) installed in Oklahoma, New Mexico, Texas, and Colorado could be used. LMAs provide lightning aloft data similar to the LDAR system, allowing predictors to be examined for all types of lightning. However, since those studies would require data from different WSR-88D sites, individual radar Z_{DR} biases would have to be taken into account when establishing and comparing Z_{DR} based predictors.

Finally, the data and results obtained from this study could be extended to a lightning cessation study. In addition to forecasting lightning initiation, 45 WS must determine when a lightning threat no longer exists. Air Force guidance currently requires that a thunderstorm be reported at a location until 15 min after the last lightning strike occurred. This can lead to long periods of interrupted operations, even if a storm has dissipated or moved away. Creating empirical guidance for lightning cessation based on DP radar could allow forecasters to accurately predict when a lightning threat no longer exists. Lightning cessation studies by Wolf (2006) and Preston and Fuelberg (2012) serve as potential starting points for cessation research focused over the 45 WS areas of responsibility.

Appendix A. 2D and 3D LDAR Visuals

This section provides four visual representations of LDAR data used for this study. The first three figures were created for the same 30 min period in June 2012, and were plotted using MATLAB®. The final figure displays the visual LDAR output as seen by forecasters at 45 WS. Each of these figures demonstrate the wealth of information that LDAR provides.

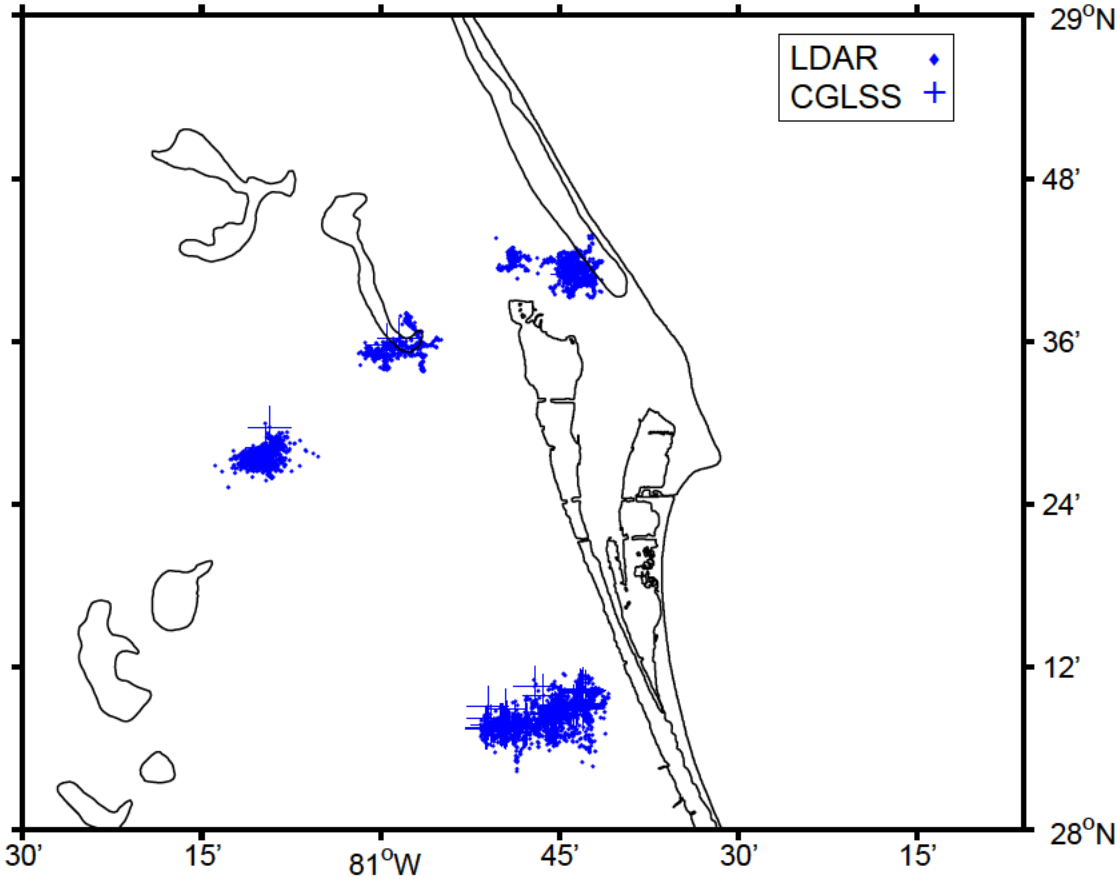

Figure 24. All LDAR results within 50 km of KSC plotted using X (east/west) and Y (north/south) coordinates for a 30 min period on 5 June 2012. This time period had four separate lightning-producing cells and close to 100 separate lightning flashes.

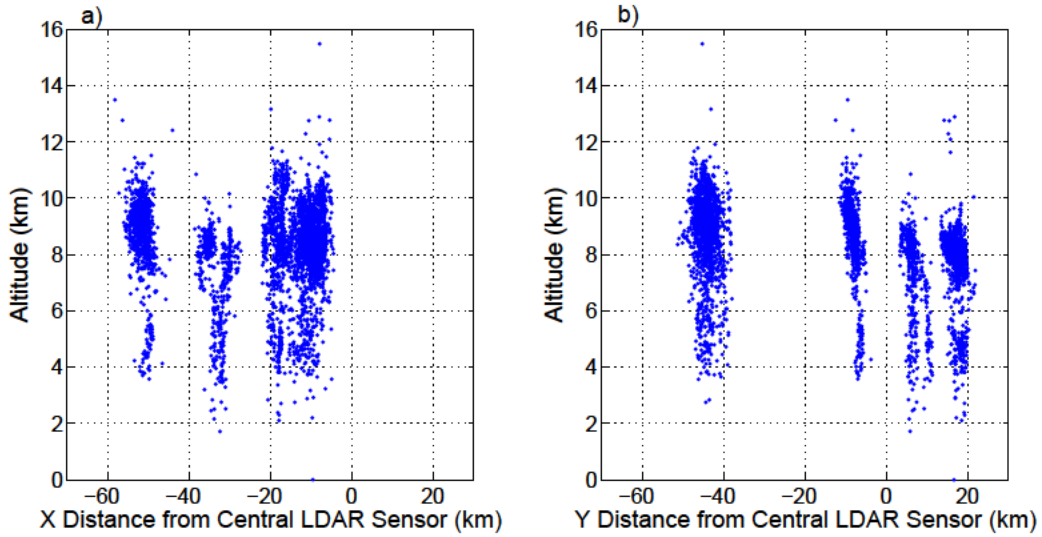

Figure 25. The same LDAR results presented in Figure 24, except Figure (a) is plotted using XZ coordinates and Figure (b) uses YZ coordinates. These figures show how LDAR uses stepped leader detection to examine the vertical orientation of a lightning flash. Many of the flashes appear vertical and represent CG lightning, but numerous flashes aloft are present and could be more easily discerned if these figures were plotted for a shorter time period.

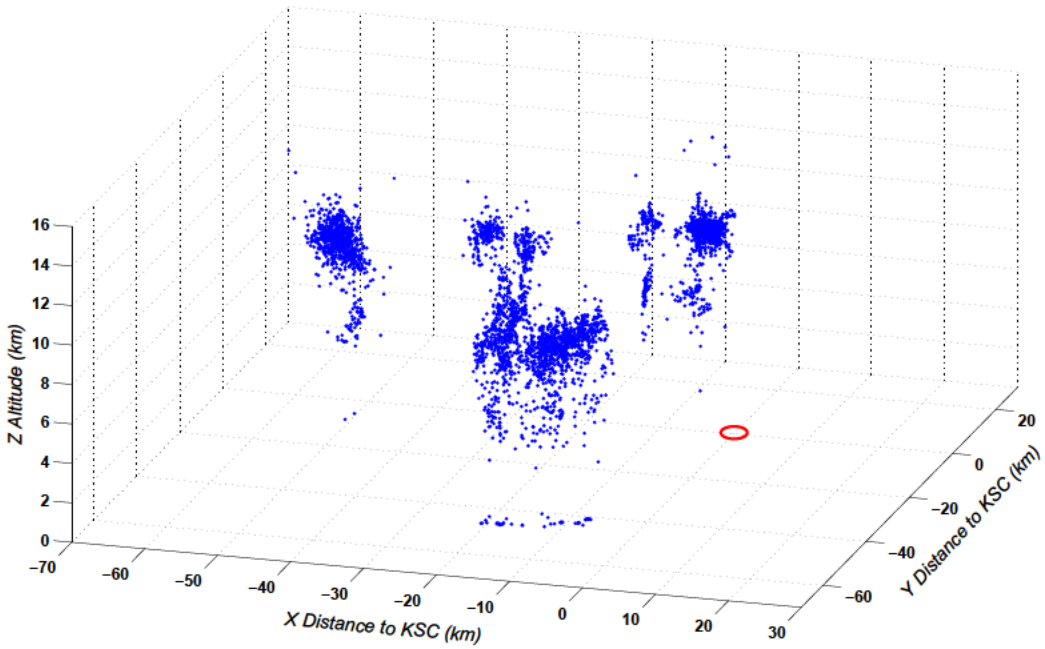

Figure 26. An LDAR plot from the same time period used in Figure 24. This plot uses the X, Y, and Z results from LDAR to create a 3-D view of stepped leaders and corresponding lightning flashes. Results where Z=0 represent CGLSS data. The red circle identifies the location of the central LDAR sensor at KSC.

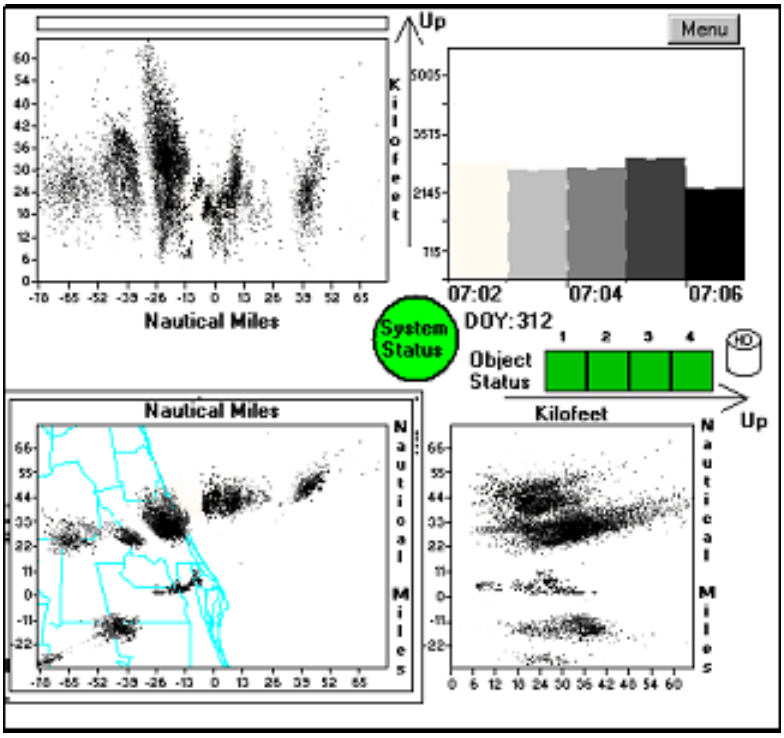

Figure 27. Screenshot of the LDAR display used by forecasters at 45 WS. This is a different event than what is shown in the three previous images. Figure provided by Roeder (2015) and used by permission.

Appendix B. Monthly and Three-Hourly Breakdown of Training and Validation Datasets

This section displays the seasonal and daily variability of convective cells examined in study. Figures 28 and 29 display monthly distributions that reveal convective cells and any associated airmass thunderstorms are most common during the summer months, which is due to intense low-level heating. Additionally, no convective cells were analyzed during January or December due to a combination of low thunderstorm frequency, radar downtime, and several LDAR outages. Figures 30 and 31 show that convective cells and any associated thunderstorms are most common during the afternoon hours. This is due to a combination of daytime heating and a corresponding enhancement in sea breeze intensity.

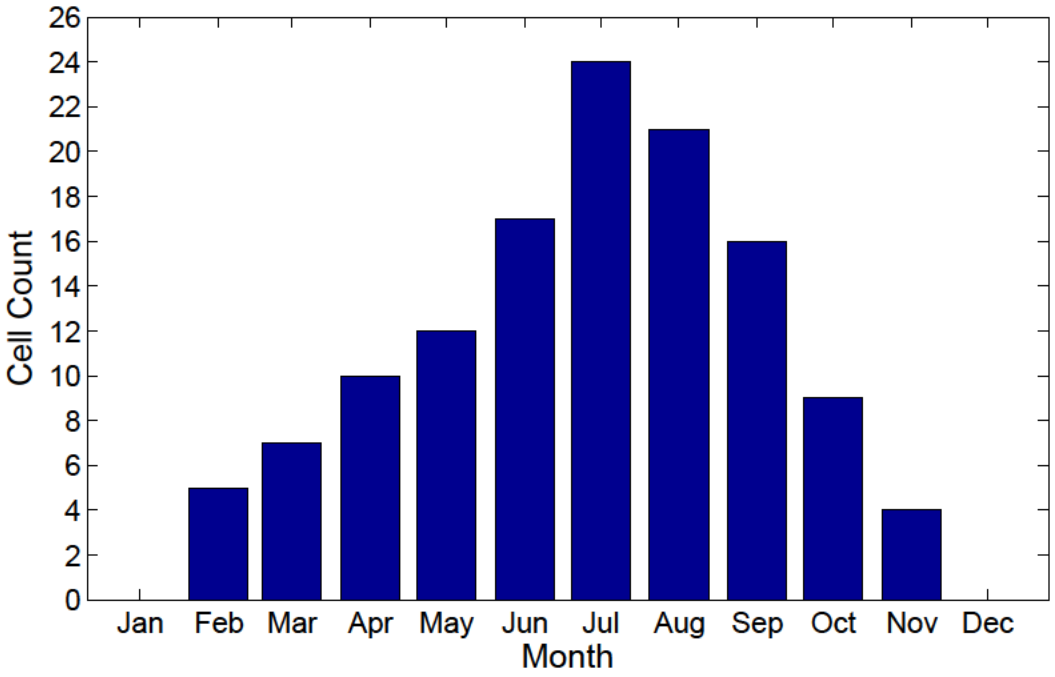

Figure 28. Monthly distribution of cells used in the training dataset.

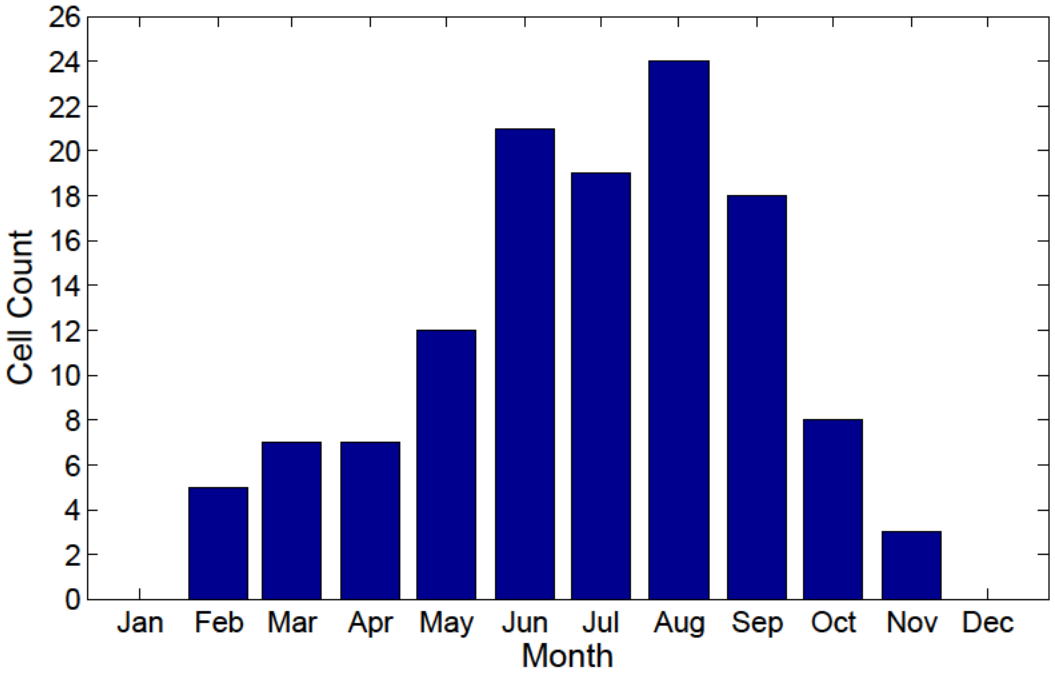

Figure 29. Monthly distribution of cells used in the validation dataset.

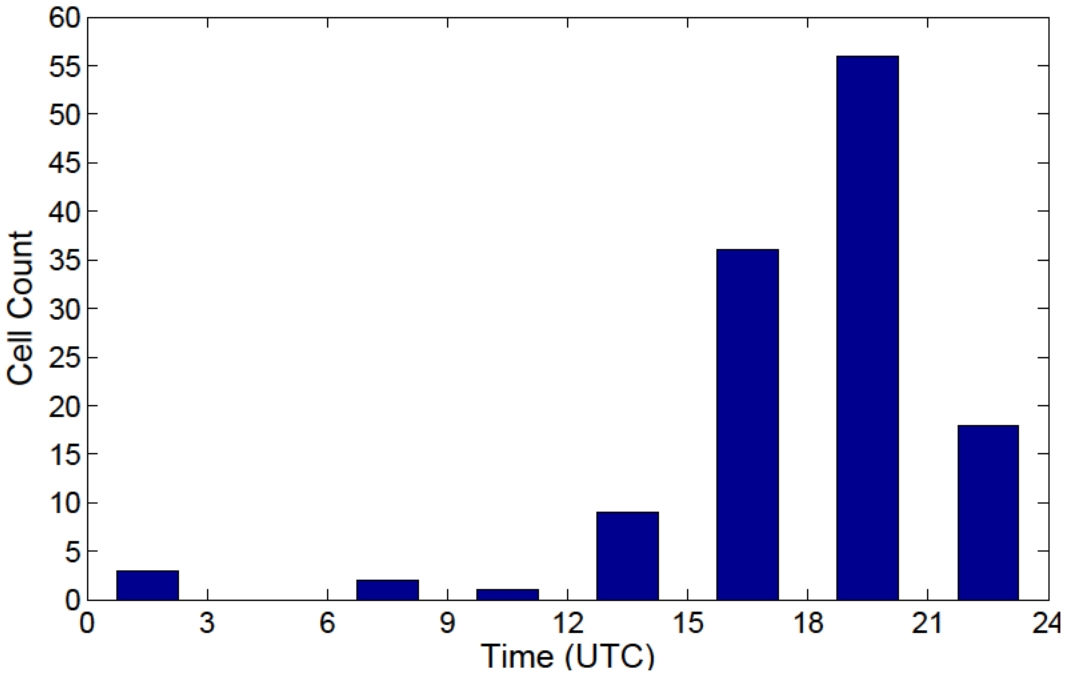

Figure 30. UTC times of cells analyzed as part of the training dataset.

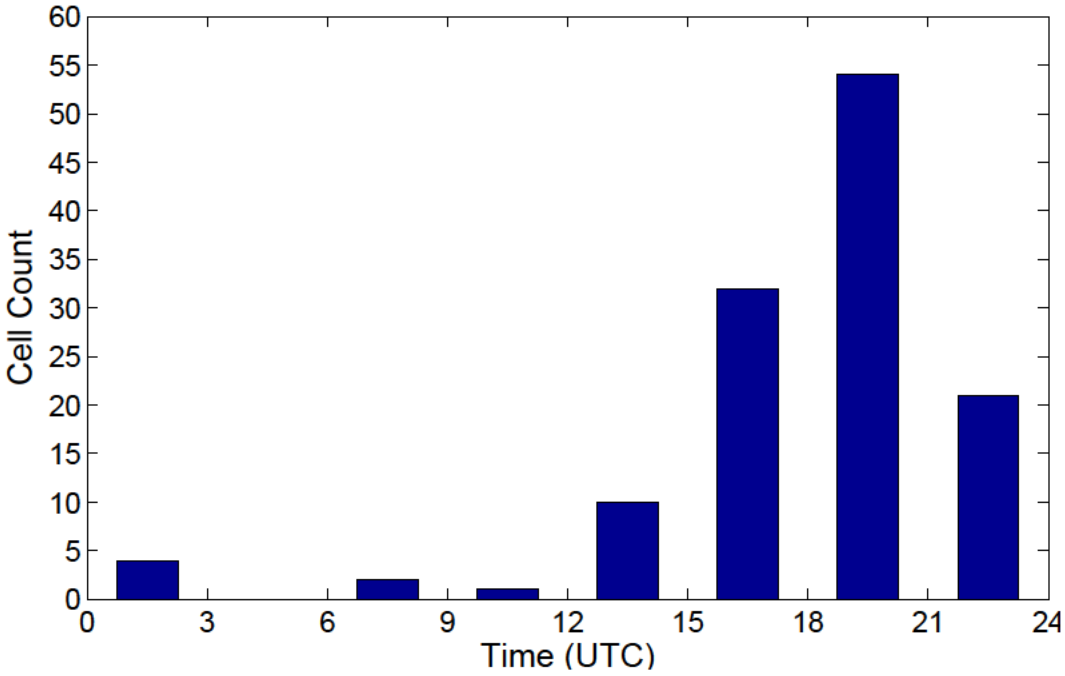

Figure 31. UTC times of cells analyzed as part of the validation dataset.

References

Beasley, W. H., D. E. Williams, and P. T. Hyland, 2008: Analysis of surface electric-filed contours in relation to cloud-to-ground lightning flashes in air-mass thunderstorms at the Kennedy Space Center. 20th International Lightning Detection Conference.

Bringi, V. N., and V. Chandrasekar, 2001: *Polarimetric Doppler Weather Radar: Principles and applications*. Cambridge University Press, Cambridge, UK.

Bringi, V. N., K. Knupp, A. Detwiler, L. Liu, I. J. Caylor, and R. A. Black, 1997: Evolution of a Florida thunderstorm during the convection and precipitation/electrification experiment: The case of 9 August 1991. *Mon. Wea. Rev.*, **125**, 2131–2160.

Bringi, V. N., T. A. Seliga, and K. Aydin, 1984: Hail detection with a differential reflectivity radar. *Science*, **225**, 1145–1157.

Buechler, D. E., and S. J. Goodman, 1990: Echo size and asymmetry: Impact on NEXRAD storm identification. *J. Appl. Meteor.*, **29**, 962–969.

Byers, H. R., and R. R. Braham Jr., 1948: Thunderstorm structure and circulation. *J. Meteor.*, **5 (3)**, 71–86.

Carey, L. D., and S. A. Rutledge, 2000: The relationship between precipitation and lightning in tropical island convection: A C-band polarimetric radar study. *Mon. Wea. Rev.*, **128**, 2687–2710.

Cummins, K. L., M. J. Murphy, E. A. Bardo, W. L. Hiscox, R. B. Pyle, and A. E. Pifer, 1998: A combinded toa/mdf technology upgrade of the u.s. national lightning detection network. *J. Geophys. Res.*, **103 (D8)**, 9035–9044.

da Silva Ferro, M. A., J. Yamasaki, D. R. M. Pimentel, K. P. Naccarato, and M. M. F. Saba, 2011: Lightning risk warnings based on atmospheric electric field measurements in Brazil. *J. Aerospace Tech. Mgmt.*, **3 (3)**, 301–310, doi:10.5028.

Dye, J. E., J. J. Jones, and D. W. Breed, 1989: The electrification of New Mexico thunderstorms. Part 1: Relationship between precipitation development and the onset of electrification. *J. Geophys. Res.*, **94**, 8643–8656.

Eastern Range Instrumentation Handbook, 2003: *Meteorological/C-CAFS/81900/LPLWS*.

Forbes, G. S., 1993: Lightning studies using LDAR and LLP data. URL https://archive.org/details/nasa_techdoc_19940018765.

Gremillion, M. S., and R. E. Orville, 1999: Thunderstorm characteristics of cloud-to-ground lightning at the Kennedy Space Center, Florida: A study of lightning initiation signatures as indicated by the WSR-88D. *Wea. Forecasting*, **14**.

Hall, M. P. M., J. W. F. Goddard, and S. M. Cherry, 1984: Identification of hydrometeors and other targets by dual-polarization radar. *Radar Science*, **19**, 132–140.

Hondl, K. D., and M. D. Eilts, 1994: Doppler radar signatures of developing thunderstorms and their potential to indicate the onset of cloud-to-ground lightning. *Mon. Wea. Rev.*, **122**, 1818–1836.

Illingworth, A. J., J. W. F. Goddard, and S. M. Cherry, 1987: Polarization radar studies of precipitation development in convective storms. *Quart. J. Roy. Meteor. Soc.*, **113**, 343–354.

Insurance Information Institute, 2014: Number, cost of homeowners insurance claims from lightning fell in 2013; dry conditions, fewer powerful thunderstorms a contributing factor. URL http://www.iii.org/press-release.

Jayaratne, E. R., C. P. R. Saunders, and J. Hallett, 1983: Laboratory studies of the charging of soft-hail during ice crystal interactions. *Quart. J. Roy. Meteor. Soc.*, **109 (461)**, 609–630.

Johnson, J. T., P. L. MacKeen, A. Witt, E. D. Mitchell, E. M. D. Stumpf, G. J. and, and K. W. Thomas, 1998: The storm cell identification and tracking algorithm: An enhanced WSR-88D algorithm. *Wea. Forecasting*, **13**, 263–276.

Jolliffe, I. T., and D. B. Stephenson, 2003: *Forecast Verification: A Practitioners Guide in Atmospheric Science*. John Wiley and Sons, West Sussex, UK.

KSC, 2014: Spaceport weather archive. URL http://kscwxarchive.ksc.nasa.gov/.

Kumjian, M. R., 2013a: Principles and application of dual-polarization weather radar. Part I: Description of the polarimetric radar variables. *J. Operational Meteor.*, **1 (19)**, 226–242.

Kumjian, M. R., 2013b: Principles and application of dual-polarization weather radar. Part II: Warm- and cold-season applications. *J. Operational Meteor.*, **1 (20)**, 243–264.

Larsen, H. R., and E. J. Stansbury, 1974: Association of lightning flashes with precipitation cores extending to height 7 km. *J. Atmos. Terr. Phys.*, **36**, 1547–1558.

MacGorman, D. R., and W. D. Rust, 1998: *The Electrical Nature of Storms*. Oxford University Press, New York, NY.

Mata, C. T., and J. G. Wilson, 2012: Future expansion of the lightning surveillance system at the kennedy space center and the cape canaveral air force station, florida, usa. 22nd International Lightning Detection Conference.

Michimoto, K., 1991: A study of radar echoes and their relationship to lightning discharge of thunderclouds in the Hokuriku District. Part I: Observation and analysis of thunderclouds in summer and winter. *J. Meteor. Soc. Japan*, **69**, 327–335.

Mosier, R. M., C. Schumacher, R. E. Orville, and L. D. Carey, 2011: Radar nowcasting of cloud-to-ground lightning over Houston, Texas. *Wea. Forecasting*, **26**, 199–212.

Murphy, M. J., K. L. Cummins, N. W. S. Demetriades, and W. P. Roeder, 2008: Performance of the new four-dimensional lightning surveillance system (4dlss) at the kennedy space center/cape canaveral air force station complex. 13th Conference on Aviation, Range and Aerospace Meteorology.

Murray, N. D., E. P. Krider, and J. E. Dye, 2005: Surface observations of the electric field and the radar reflectivity of decaying thunderstorm anvils and debris clouds at the NASA Kennedy Space Center. Conference on Meteorological Applications of Lightning Data.

NASA, 2014: Nasa missions. URL http://www.nasa.gov/missions/.

NCDC, 2014: Radar data access. URL http://www.ncdc.noaa.gov/oa/radar/radardata.html.

NHC, 2014: NHC data archive. URL http://www.nhc.noaa.gov/data/.

NOAA, 2012: Melbourne WSR-88D dual-polarization upgrade. URL http://www.srh.noaa.gov/mlb/?n=dualpol.

NOAA, 2014: NWS lightning safety. URL http://www.lightningsafety.noaa.gov/.

NWS, 2014: Radar operations center. URL http://www.roc.noaa.gov/WSR88D/.

Plymouth State Weather Center, 2014: Archived radar control message data maps. URL http://vortex.plymouth.edu/rcm-u.html.

Preston, A. D., and H. E. Fuelberg, 2012: The use of polarimetric radar data in determining lightning cessation. 22nd International Lightning Detection Conference.

Rakov, V. A., and M. A. Uman, 2003: *Lightning: Physics and Effects*. Cambridge University Press, Cambridge, UK.

Reynolds, S. E., M. Brook, and M. F. Gourley, 1957: Thunderstorm charge separation. *J. Meteor.*, **14**, 426–436.

Rinehart, R. E., 2010: *Radar for Meteorologists*. Rinehart Publishing, Neveda, MO.

Roeder, W. P., 2010: The four dimensional lightning surveillance system. 21st International Lightning Detection Conference.

Roeder, W. P., 2012: Four dimensional lightning surveillance system: Status and plans. 22nd International Lightning Detection Conference.

Roeder, W. P., 2015: Personal correspondence.

Roeder, W. P., L. L. Huddleston, W. H. Baunam III, and K. B. Doser, 2014: Weather research requirements to improve space launch from Cape Canaveral Air Force Station and NASA Kennedy Space Center. Space Traffic Management Conference.

Roeder, W. P., and T. M. McNamara, 2006: A survey of the lightning launch commit criteria. 2nd Conference on Meteorological Applications of Lightning Data.

Roeder, W. P., T. M. McNamara, B. F. Boyd, and F. J. Merceret, 2009: The new weather radar for America's space program in Florida: An overview. 34th Conference on Radar Meteorology.

Roeder, W. P., and C. S. Pinder, 1998: Lightning forecasting techniques for Central Florida in support of America's space program. 16th Conference on Weather Analysis and Forecasting.

Roeder, W. P., J. W. Weems, and P. B. Wahner, 2005: Applications of the cloud-to-ground lightning surveillance system database. Conference on Meteorological Applications of Lightning Data.

Rogers, R. R., and M. K. Yau, 1989: *A Short Course in Cloud Physics*. 3rd ed., Butterwoth-Heinemann, Oxford, UK.

Starr, S., D. Sharp, F. Merceret, J. Madura, and M. Murphy, 1993: LDAR, a three-dimensional lightning warning system : Its development and use by the government, and transition to public availability.

Thurmond, K. R., 2014: Operational cloud-to-ground lightning initiation forecasting utilizing s-band dual-polarization radar. M.S. thesis, Air Force Institute of Technology.

Vaisala, 2013: Vaisala national lightning detection network. URL http://www.vaisala.com/en/products/thunderstormandlightningdetectionsystems/Pages/NLDN.aspx.

Vincent, B. R., L. D. Carey, D. Schneider, K. Keeter, and R. Gonski, 2003: Using WSR-88D reflectivity data for the prediction of cloud-to-ground lightning: A North Carolina study. *Natl. Weather Dig.*, **27**, 35–44.

Wallace, J. M., and P. V. Hobbs, 2006: *Atmospheric Science: An Introductory Survey*. 2nd ed., Academic Press, San Diego, CA.

Wolf, P., 2006: Anticipating the initiation , cessation , and frequency of cloud-to-ground lightning , utilizing WSR-88D reflectivity data. *J. Operational Meteor.*, **1 (20)**.

Woodard, C. J., 2011: Operational lightning forecasting technique development and testing utilizing c-band dual-polarimetric radar. M.S. thesis, University of Alabama in Huntsville.

Woodard, C. J., L. D. Carey, W. A. Petersen, and W. P. Roeder, 2012: Operational utility of dual-polarization variables in lightning initiation forecasting. *J. Operational Meteor.*, **13 (6)**.

Wyoming Weather Web, 2014: Upper air data. URL http://weather.uwyo.edu/upperair/.

Yang, Y. H., and P. King, 2010: Investigating the potential of using radar echo reflectivity to nowcast cloud-to-ground lightning initiation over Southern Ontario. *Wea. Forecasting*, **25 (4)**, 1235–1248.

Vita

Captain Andrew Travis was born in Dunkirk, New York, but primarily grew up in Maine and New Hampshire. Upon graduating from Oyster River High School in Durham, New Hampshire in 2001, he attended the University of New Hampshire and joined the Reserve Officer Training Corps, Detachment 475. In 2002, he transferred to Plymouth State University to pursue a degree in meteorology. In May 2006, he graduated summa cum laude with a Bachelor of Science Degree in Meteorology with minors in Mathematics and Economics. Upon graduation, he was commissioned as a Second Lieutenant in the United States Air Force.

Captain Travis' first assignment was at the 25th Operational Weather Squadron, Davis-Monthan AFB, Arizona. There he served in various positions before rising to the position of Senior Duty Officer. In 2010, he completed a PCS to the 31st Operations Support Squadron, Aviano AB, Italy where he served as a Wing Weather Officer, Flight Commander, and Operations Group Executive Officer. During this assignment, he supported Operations ODYSSEY DAWN and UNIFIED PROTECTOR over Libya, and he also served six months as the Third Army Staff Weather Officer at US Army Central, Camp Arifjan, Kuwait. While stationed in Italy, he earned a Master of Science Degree in Management with Distinction from Embry-Riddle Aeronautical University.

In May 2013, Capt Travis entered the Graduate School of Engineering Management at the Air Force Institute of Technology, Wright-Patterson AFB, Ohio to obtain a Master's Degree in Applied Physics with a specialization in Atmospheric and Space Sciences. Upon graduation, he will be assigned to the 335th Training Squadron at Keesler AFB, Mississippi to instruct the Weather Officer Course.

REPORT DOCUMENTATION PAGE

Form Approved
OMB No. 0704–0188

1. REPORT DATE *(DD–MM–YYYY)*	2. REPORT TYPE	3. DATES COVERED *(From — To)*
26-03-2015	Master's Thesis	May 2013 — Mar 2015

4. TITLE AND SUBTITLE

Utilizing Four Dimensional Lightning and Dual-Polarization Radar to Develop Lightning Initiation Forecast Guidance

5a. CONTRACT NUMBER

5b. GRANT NUMBER

5c. PROGRAM ELEMENT NUMBER

6. AUTHOR(S)

Travis, Andrew J., Captain, USAF

5d. PROJECT NUMBER

5e. TASK NUMBER

5f. WORK UNIT NUMBER

7. PERFORMING ORGANIZATION NAME(S) AND ADDRESS(ES)

Air Force Institute of Technology
Graduate School of Engineering and Management (AFIT/EN)
2950 Hobson Way
WPAFB OH 45433-7765

8. PERFORMING ORGANIZATION REPORT NUMBER

AFIT-ENP-MS-15-M-092

9. SPONSORING / MONITORING AGENCY NAME(S) AND ADDRESS(ES)

45th Weather Squadron
1201 Edward H. White Ste. C-129
Patrick AFB, FL 32925
COMM: (321) 853-8410
Email: william.roeder@us.af.mil

10. SPONSOR/MONITOR'S ACRONYM(S)

45 WS

11. SPONSOR/MONITOR'S REPORT NUMBER(S)

12. DISTRIBUTION / AVAILABILITY STATEMENT

DISTRIBUTION STATEMENT A: APPROVED FOR PUBLIC RELEASE; DISTRIBUTION UNLIMITED.

13. SUPPLEMENTARY NOTES

14. ABSTRACT

Lightning initiation is a major forecast challenge faced by Air Force's 45th Weather Squadron (45 WS), which provides weather support to Cape Canaveral Air Force Station and Kennedy Space Center (KSC). Prior studies by Thurmond (2014) and Woodard (2011) have shown that dual-polarization (DP) radar can be used to identify the presence of hydrometeors indicative of cloud charging, leading to improved lightning initiation forecasts. The 45 WS currently employs empirical lightning initiation forecast rules which state that in-cloud lightning is likely when radar reflectivity meets or exceeds 37.0 dBZ above the $-10°$C height. This study examined 249 convective cells from March 2012 to March 2014 in order to incorporate DP parameters into existing forecast principles. In-cloud and cloud-to-ground lightning flash data were obtained from the KSC Four Dimensional Lightning Surveillance System, and DP data were obtained from the Melbourne, Florida WSR-88D. Lightning initiation forecast lead times, probabilities of detection, and false alarm rates were compared between candidate DP-based forecast techniques and techniques employed by 45 WS.

15. SUBJECT TERMS

Forecasting Lightning, Dual-Polarization, Weather Radar, Lightning Detection, 45th Weather Squadron

16. SECURITY CLASSIFICATION OF:			17. LIMITATION OF ABSTRACT	18. NUMBER OF PAGES	19a. NAME OF RESPONSIBLE PERSON
a. REPORT	b. ABSTRACT	c. THIS PAGE			Lt Col Robert S. Wacker, AFIT/ENP
U	U	U	UU	91	19b. TELEPHONE NUMBER *(include area code)* (937) 255-3636, x4609; robert.wacker@afit.edu